의학박사 학위논문

Effects of low-dose bisphenol A on transcriptional expression of breast cancer cell lines, tumor immunity, and cancer progression

저용량 비스페놀A 노출이 유방암 세포의 전사체 발현, 종양면역 및 암 진행에 미치는 영향에 관한 연구

2020년 8월

서울대학교 대학원

의과학과

김혜림

A Thesis of the Degree of Doctor of Philosophy

저용량 비스페놀 A 노출이 유방암 세포의 전사체 발현, 종양면역 및 암 진행에 미치는 영향에 관한 연구

Effects of low-dose bisphenol A on transcriptional expression of breast cancer cell lines, tumor immunity, and cancer progression

August 2020

The Department of Biomedical Sciences,

Seoul National University

College of Medicine

HYELIM KIM

ABSTRACT

Effects of low-dose bisphenol A on transcriptional expression of breast cancer cell lines, tumor immunity, and cancer progression

HYELIM KIM

Biomedical Sciences
The Graduate School
Seoul National University

Introduction: Bisphenol A (BPA) used in the manufacture of polycarbonate plastics and epoxy resin has structurally estrogen-like activity and recent studies have indicated that exposure to BPA in environment and daily life may account for the increased incidence of breast cancer in the industrialized world. Multiple in vivo and in vitro studies have reported that BPA exposure at low doses can result in breast neoplastic lesions. However, the correlation among BPA exposure, transcriptional alterations in breast cancer cells and breast cancer progression is not fully elucidated. In this study, we investigated whether chronic exposure to low-dose BPA affects transcriptome expression alterations and malignancy in different subtypes of breast cancer cells and mouse xenograft models.

Methods: This study consists of two independent experiments.

1. ER-positive MCF-7, HER2-enriched SK-BR3, triple-negative MDA-MB-231 cells were used as breast cancer cell lines according to hormone receptor status. We analyzed the RNA-sequencing data from breast cancer cells treated with BPA at a low dose (10^{-8} M) for 30 days. Sequencing libraries were constructed using a QuantSeq 3' mRNA-Seq Library Prep Kits. Differentially expressed genes (DEGs) were determined using BEDtools following mapping libraries using Bowtie2 software. Functional analysis was conducted by online public database DAVID, KEGG and PANTHER etc. Moreover, a functionally organized network of DEGs belonging to among MCF-7/BPA, SK-BR3/BPA and MDA-MB-231/BPA cells was created using the Cytoscape software platform. Afterward, we analyzed the correlation between BPA-exposed DEGs and survival rate of patients with various subtypes of breast cancer using public database BreastMark.

2. We investigated the effects of BPA (10^{-8} M) on the regulation of MCF10DCIS.com cells, ductal carcinoma in situ (DCIS), considered early-stage breast cancer and of RAW264.7, macrophages, the most abundant population in tumor immune microenvironment to determine the DCIS progression to invasive metastasis. The effects of BPA exposure on MCF10DCIS.com cell proliferation and migration abilities were evaluated by MTT and Trans-well migration assays with 0.8 μm pore size. In addition, intracellular signaling pathways related to these abilities were analyzed by Western blotting. Immune function analysis of BPA-exposed macrophages was performed using real-time RT-PCR and western blot. Moreover, we evaluated interactions between breast

cancer cells and macrophages through co-culture method with conditioned medium for 72 h or with trans-well chambers with 0.4 μm pore size. Tumor xenograft models for early-stage breast cancer were established by injection with DCIS.com/Luc-GFP cells into the second fat pad of mice after exposure to BPA (10^{-8} M) for 30 days via drinking water of immune deficient mice (BALB/c nude mice) at 3 weeks of age. We monitored tumor progression and metastasis with bioluminescence imaging. Afterward, we evaluated metastasis and immune function of tumor-associated macrophages by immunohistochemistry with macrophage marker F4/80, inflammatory M1 marker NOS2, protumorigenic M2 marker CD206 in lymph node tissues surrounding tumors as well as primary tumors, and CK5 for identifying metastatic breast cancer cells in lymph node tissues surrounding tumors.

Result: 1. We confirmed common changes in immune functions such as NKT, NK and T cell activation and dendritic cell migration by transcriptome expression analysis across MCF-7, SK-BR3, MDA-MB-231 cells affected by chronic exposure to low-dose BPA. The high expression of immune-related genes (IL19, CA9, and SPARC) under BPA exposure was associated with decreased overall survival in patients with breast cancer.

2. In the same manner, results of the transcriptional analysis of MCF10DCIS.com cells exposed to BPA showed immune-related alterations. BPA exposure promoted proliferative and migratory abilities of MCF10DCIS.com cells and induced polarization of RAW264.7 cells toward the M1/M2 phenotypes with high expression of NOS2, arginase-1, and CD206.

Chronic low-dose BPA exposure group showed induction of M2 phenotype tumor-associated macrophages surrounding primary tumor, and were promoted tumor growth and lymph node metastasis in mouse model for breast cancer, as well.

Conclusions: 1. These findings indicate chronic low-dose BPA exposure has dissimilar impacts on the regulation of gene expression and diverse biological functions, including immune modulation, in different subtypes of breast cancer cell.

2. These results demonstrate that BPA acts as an accelerator to promote DCIS progression to invasive breast cancer by affecting DCIS cell proliferation and migration as well as macrophage polarization toward a protumorigenic phenotype.

Key words: Bisphenol A, Breast cancer, Macrophage polarization, Transcriptional analysis, Tumor progression

Student Number: 2015-22030

CONTENTS

LIST OF TABLES

LIST OF FIGURES

LIST OF ABBREVIATIONS

BPA－Bisphenol A

BCC－Breast cancer cell

EDC－Endocrine-disrupting chemical

RNA－seq－RNA sequencing

DEG－Differentially Expressed Gene

GO－Gene Ontology

KEGG－Kyoto Encyclopedia of Genes and Genomes

DAVID－Database for Annotation Visualization and Integrated Discovery

BP－Biological process

CC－Cellular component

MF－Molecular function

OS－Overall survival

HR－Hazard ratio

OS－ Overall survival

LN－ Lymph node

DCIS－Ductal carcinoma in situ

Chapter 1

Comparison of transcriptome expression alterations by chronic exposure to low-dose bisphenol A in different subtypes of breast cancer cells

INTRODUCTION

Endocrine-disrupting chemicals (EDCs) can interfere with endocrine systems [1]. Bisphenol A (BPA) is a known estrogen-mimicking EDC to which most people in the industrialized world are exposed [2]. There is evidence for the possible involvement of BPA in genetic and epigenetic endocrine and immune disruption through diverse cellular and molecular mechanisms, eventually leading to the alteration of gene profiles and the induction of chronic disease in humans [3,4]. Due to these potential harmful effects caused by BPA, recent studies have raised serious concerns about the deleterious impacts of BPA on the induction or promotion of human diseases, including cancer [5]. Chronic exposure to BPA at a low dose has been suggested to be a potential risk factor for inducing breast cancer and accelerating the progression of aggressive breast cancers [6–10]. The effects of BPA vary with the dose and time of exposure in a nonmonotonic dose-response manner characterized by stimulation at low doses and inhibition at high doses [11,12]. The low concentrations of BPA to which adults are exposed are no > 0.4-1.5 μg of BPA/kg/day, and 95% of BPA exposures are unlikely to exceed 1.5-4.2 μg of BPA/kg/day [13]. A low dose of BPA (10^{-8} M in vitro and 2.5 μg/L in vivo) is within a safe reference dose for humans according to the guidelines of the U.S. Environmental Protection Agency (EPA) and the Food and Drug Administration (FDA) [12,14]. We previously reported that chronic exposure to BPA at an environmentally human-relevant low dose acts as an accelerator to increase the aggressiveness of ductal carcinoma in situ breast cells through immune modulation

[15]. Given this background, the multiple effects of BPA, including those on immune function in different subtypes of breast cancer cells (BCCs), have attracted much attention, with particular interest in chronic exposure to low doses of BPA.

Breast cancer, which is a heterogeneous complex of diseases, is divided into four major molecular subtypes-hormone receptor-positive luminal A and B, human epidermal growth factor receptor 2 (HER2)-enriched and triple-negative (TN) - that are based on the gene expression profile and the classical immunohistochemical markers, hormone receptors, the estrogen receptor (ER) and/or progesterone receptor (PR), and HER2 [16]. An epidemiological study suggested a link between BPA exposure and the progression of aggressive breast cancer subtypes [17]. BCCs with distinct molecular subtypes differentially respond to drugs or chemicals. There is evidence of heterogeneous immunogenicity in specific subtypes of breast cancer, such as HER2-enriched and TN breast cancers [18,19]. Due to differences in the features and biological behaviors of BCCs, comparing the deleterious impact of BPA between the subtypes of BCCs is essential for the development of new strategies to treat breast cancer patients environmentally or occupationally exposed to BPA.

Transcriptome profiling performed by RNA sequencing (RNA-seq) has been used to uncover multiple molecular mechanisms and explore diagnostic and predictive biomarkers [20]. To the best of our knowledge, the global gene expression and the pathway networks altered by chronic exposure to BPA at low

doses have not been investigated in the different subtypes of BCCs. In this study, the transcriptome expression profiles, Gene Ontology (GO) term and pathway enrichment, and immune network in BPA-exposed BCC lines classified as the luminal A, HER2-enriched and TN subtypes were analyzed, and the BCC subtype-specific and detrimental gene signatures were explored to predict the prognostic significance linked to BPA exposure.

MATERIALS AND METHODS

Human BCC lines and BPA exposure

The human BCC lines MCF-7 (ER+/PR+/HER2-), SK-BR3 (ER-/PR-/HER2+), and MDA-MB-231 (ER-/PR-/HER2-) were purchased from the Korean Cell Line Bank (Seoul, Korea). MCF-7 and SK-BR3 cells were grown in Dulbecco's modified Eagle's medium (DMEM) (WelGENE, Daegu, Korea) containing 10% fetal bovine serum (FBS) and supplemented with 1% penicillin and streptomycin (Gibco, Langley, OK, USA). MDA-MB-231 cells were cultured in Roswell Park Memorial Institute (RPMI) 1640 medium (WelGENE) containing 10% FBS and supplemented with a 1% antibiotic solution containing penicillin and streptomycin (Gibco). All cell lines were cultured in a humidified atmosphere with 5% CO_2 at 37℃.

BPA (Sigma-Aldrich, St. Louis, MO, USA) was dissolved in 0.1% dimethyl sulfoxide (DMSO, Sigma-Aldrich). The BPA-exposed cell groups were acquired by incubating BCCs in the presence of BPA. The effect of BPA was compared to that of 0.1% DMSO (control).

Proliferation assay

Cells (5×10^3) were seeded in a 96-well plate and incubated in culture medium for 24 h. BPA (10^{-10}-10^{-4} M) was administered to cells for 24-72 h. Briefly, 3-(4,5-dimethylthiazol-2-yl)-2,5-diphenyltetrazolium bromide (MTT) reagent

(250 μg/mL) was added to each well and incubated for 1 h at 37℃. Formazan crystals were solubilized by the addition of 150 μl of DMSO to each well. The optical density at 540 nm was measured by using a microplate reader (Bio-Rad Laboratories, Inc., Hercules, CA, USA), and the cell proliferation rate was determined.

RNA isolation and RNA-seq

Total RNA was extracted from BCCs using TRIzol reagent (Invitrogen, Carlsbad, CA, USA) according to the manufacturer's instructions. The RNA concentration was measured using a NanoDrop 2000 spectrophotometer (Thermo Fisher Scientific, Inc., Waltham, MA, USA). The RNA integrity number (RIN) was determined utilizing an Agilent RNA 6000 Nano kit following the manufacturer's protocol on an Agilent 2100 bioanalyzer (Agilent, Santa Clara, CA, USA).

Sequencing libraries were constructed using a QuantSeq 3′ mRNASeq Library Prep Kit (Lexogen, South Morang Victoria, Australia) according to the manufacturer's instructions. High-throughput RNA-seq was performed by single-end 75-bp sequencing using a NextSeq 500 system (Illumina, San Diego, CA, USA). The differentially expressed genes (DEGs) between BPA-exposed BCCs and control cells were determined based on counts from unique and multiple alignments using coverage in BEDtools (Quinlan and Hall, 2010). The read count (RC) data were processed based on the quantile normalization method via the EdgeR package within R using Bioconductor [21]. To select DEGs, we ranked

genes with a p-value of < 0.05 by the log10 p-value and plotted them against the log2-fold change (FC) in a volcano plot. Upregulated and downregulated genes with a p-value of < 0.05 and a log2FC ratio of > 0.59 were identified.

GO and Kyoto Encyclopedia of Genes and Genomes (KEGG) pathway enrichment and immune network analyses

To gain insight into the underlying biology of DEGs modulated by chronic exposure to 10^{-8} M BPA, biological functional categories enriched in the DEGs were identified using the functional annotation and clustering tool of the Database for Annotation, Visualization, and Integrated Discovery v6.7 (DAVID, https://david.ncifcrf.gov/). The significant GO terms were identified after adjustment for multiple testing with the Benjamini Hochberg method; a Benjamini adjusted p-value of < 0.05 was considered to indicate a statistically significant difference. Functional categories were considered enriched when the log scale geometric mean had a p-value of < 0.05 (enrichment score $\geq$ 1.3). GO term lists [biological process (BP); cellular compartment (CC); molecular function (MF)] were matched with each other. Additionally, GO terms were searched using the web-based tool QuickGO (https://www.ebi.ac.uk/QuickGO/). To further understand the biological functions of the DEGs, KEGG pathway enrichment analysis was performed using the DAVID online tool. Additionally, PANTHER and Reactome pathways were analyzed by using the PANTHER database (http://www.PANTHERdb.org/). For identifying significant enrichment of pathways,

a Fisher's exact test with significance level set to 0.05 was used. The functionally organized immune network was created using Cytoscape software (version 3.7.1) (http://www.cytoscape.org/) with the CluePedia plugin.

Quantitative real-time RT-PCR

Several genes involved in immune and inflammatory responses were selected for quantitative real-time RT-PCR (qRT-PCR) validation. RNA was reverse transcribed using random hexamers and Superscript III reverse transcriptase. cDNA was synthesized using M-MLV reverse transcriptase (Invitrogen, USA) and random primers. Real-time PCRs were run on an ABI 7500 system utilizing SYBR Green PCR master mix (Applied Biosystems, Waltham, MA, USA) and the specific primers for IL12A, IL15, IL19, CXCL5, SERPINF2, CRIP1 and HIST1H2BE. The information for the specific primers is provided in Table 1-1. The results were analyzed by the $2^{-\Delta\Delta CT}$ method [22], which reflects the threshold difference between the expression levels of a target gene and β-actin in each sample, and the relative gene expression level was set to 1 for control cells cultured in the absence of BPA.

Enzyme-Linked Immune Sorbent Assay (ELISA)

After exposing breast cancer cells to 10^{-8} M BPA for a month, Cytokine profiles (IL19, IL15, CXCL5 and IL12A) of cell lysates of BPA-exposed breast cancer cells were evaluated by ELISA with commercially available kit (RayBiotech,

Peachtree Corners, GA, USA) according to the manufacturer's instructions.

Analysis of the BreastMark dataset

In order to examine the prognostic value of the DEGs identified in MCF-7/BPA, SK-BR3/BPA, and MDA-MB-231/BPA cells, Kaplan-Meier overall survival (OS) analyses in breast cancer were conducted using BreastMark (http://glados.ucd.ie/BreastMark/), an integrated approach to mining publicly available transcriptomic datasets relating to breast cancer outcome [23]. Briefly, Cut-off option to determine the gene expression was median; high group to the top 25% expression level and low group to the bottom 25% expression level based on the interquartile range we used to classify the breast cancer samples (SSP2006 and PAM50) into their molecular subtypes, Luminal A, Luminal B, HER2-enriched and TN. The log-rank p-value is shown for difference in survival. Cox regression analysis is used to calculate hazard ratios (HR). A HR of greater than one indicates that the marker was associated with poor prognosis, while a ratio of less than one means that it was associated with good prognosis.

Statistical analysis

Data were obtained from at least three independent experiments and are expressed as the means ± standard deviations for each group. Statistical analyses, including Student's t-test and Analysis of Variance (ANOVA), were conducted using GraphPad Prism 5.0 software (GraphPad, Inc., La Jolla, CA, USA). $p < .05$ was

considered to indicate a statistically significant difference. Only those genes with log2FC values > 0.59 and p−values < .05 were considered for bioinformatics analysis.

RESULTS

Transcriptome profiles of BPA-exposed MCF-7, SK-BR3, and MDA-MB-231 cells

To evaluate the time- or dose-dependent cytotoxic effect of BPA, MCF-7, SK-BR3, and MDA-MB-231 cells were treated with concentrations of BPA ranging from 10^{-10} to 10^{-4} M for 24 h, 48 h and 72 h, and an MTT assay was conducted. At 10^{-4} M, BPA reduced the viability of MCF-7, SK-BR3 and MDA-MB-231 cells in a time-dependent manner, whereas cell viability significantly increased after exposure of 10^{-10} to 10^{-6} M BPA (Figs. 1-1; A-C). To study the long-term exposure to BPA, 10^{-8} M BPA to maximize cancer cell growth without toxicity was chosen.

Changes in the transcriptome profiles of MCF-7, SK-BR3, and MDA-MB-231 cells treated with BPA at a low dose (10^{-8} M) for 30 days relative to those of 0.1% DMSO-treated (vehicle control) cells were identified by a QuantSeq 3' mRNA-Seq kit. The numbers of significantly (1.5-fold) up- or downregulated DEGs in MCF-7/BPA, SK-BR3/BPA, and MDA-MB-231/BPA cells relative to control cells are summarized in Figs. 1-2; A-C ($p < .05$). In MCF-7/BPA cells, a total of 172 DEGs (1.5-fold change, $p < .05$) were identified, among which 93 were upregulated and 79 were downregulated. In SK-BR3/BPA cells, a total of 137 DEGs (1.5-fold change, $p < .05$) were identified, among which 81 were upregulated and 56 were downregulated. In MDA-MB-231/BPA cells, a total of 139 DEGs

(1.5-fold change, $p < .05$) were identified, among which 56 were upregulated and 83 were downregulated. In addition, the global expression profiles of the significantly and differentially expressed genes identified in MCF-7/BPA, SK-BR3/BPA, and MDA-MB-231/BPA cells are represented in a heat map (Figs. 1-2; D-F). The top 10 up- or downregulated genes ordered by p-value and fold change in MCF-7/BPA, SK-BR3/BPA, and MDA-MB-231/BPA cells relative to control cells are shown in Tables 1-2, 1-3, and 1-4, respectively. Among the significantly (1.5-fold) up- or downregulated DEGs identified from MCF-7/BPA, SK-BR3/BPA, and MDA-MB-231/BPA cells relative to control cells, overlapping DEGs between MCF-7/BPA and SK-BR3/BPA cells (FAM209B), between MCF-7/BPA and MDA-MB-231/BPA cells (DY19L2P4, SERPINF2, CYP2S1 and PAPOLB), between SK-BR3/BPA and MDA-MB-231/BPA cells (LHX4-AS1, CRLF2, and IL12A) were identified (Fig. 1-2; G).

GO and pathway enrichment analyses of the DEGs identified from BPA-exposed MCF-7, SK-BR3, and MDA-MB-231 cells

The GO annotations for the sets of DEGs with significant cluster profiles were analyzed using the DAVID database to determine the potential functions of the DEGs. Significantly enriched GO categories with $p < .05$ were selected for analysis.

A total of six BP terms, one CC term and one MF term were significantly enriched in up- or downregulated DEGs in MCF-7/BPA cells. In upregulated DEGs of MCF-7/BPA cells, four BP terms [cellular response to gonadotropin-releasing

hormone (GO:0097211), regulation of transcription, DNA-templated (GO:0006355), intraciliary retrograde transport (GO:0035721), and chemical synaptic transmission (GO:0007268)], and one CC term [intraciliary transport particle A (GO:0030991)] were enriched (Fig. 1-3; A). In downregulated DEGs of MCF-7/BPA cells, two BP terms [brain development (GO:0007420) and negative regulation of fibrinolysis (GO:0051918)] and one MF term [lipid transporter activity (GO:0005319)] were enriched (Fig. 1-3; B).

Six BP, two CC and three MF terms in SK-BR3/BPA cells were significantly enriched in up- or downregulated DEGs. In upregulated DEGs of SK-BR3/BPA cells, two BP terms [bicarbonate transport (GO:0015701) and definitive hemopoiesis (GO:0060216)] and one CC term [extracellular region (GO:0005576)] were enriched (Fig. 1-3; C). In downregulated DEGs of SK-BR3/BPA cells, four BP terms [positive regulation of inflammatory response (GO:0050729), calcium ion transmembrane transport (GO:0070588), superoxide anion generation (GO:0042554), and signal transduction (GO:0007165)], one CC term [integral component of plasma membrane (GO:0005887)], and three MF terms [calcium channel activity (GO:0005262), superoxide-generating NADPH oxidase activity (GO:0016175), and protein homodimerization activity (GO:0042803)] were enriched (Fig. 1-3; D).

In MDA-MB-231/BPA cells, two BP terms, one CC term and one MF term were significantly enriched in only upregulated DEGs. The BP terms [negative

regulation of keratinocyte proliferation (GO:0010839) and magnesium ion transmembrane transport (GO:1903830)], CC term [platelet alpha granule (GO:0031091)], and MF term [magnesium ion transmembrane transporter activity (GO:0015095)] were enriched (Fig. 1-3; E). The detailed information on these genes belonging to the significantly enriched GO terms in MCF-7/BPA, SK-BR3/BPA, and MDA-MB-231/BPA cells is shown in Table 1-5.

In order to determine the potential pathways of the DEGs with an absolute fold change of ≥ 1.5 and a p-value of < 0.05, we used the major curated signaling pathway databases: KEGG, PANTHER and Reactome. Significantly enriched KEGG, PANTHER and Reactome pathways with $p < .05$ were selected. In MCF-7/BPA cells, a total of 4 KEGG pathways, 6 PANTHER pathways and 61 Reactome pathways were significantly enriched (Table 1-6): Choline metabolism and glutamate signaling pathways, which contributes to the aggressive behaviors of cancer cells, were significantly enriched in upregulated DEGs. Coagulation pathway frequently occurs in diverse cancer were significantly enriched in downregulated DEGs. In SK-BR3/BPA cells, there was no significantly enriched KEGG and PANTHER pathways, but a total of 70 Reactome pathways were identified (Table 1-7): VEGF/VEGFR signaling pathways were identified in upregulated DEGs. In MDA-MB-231/BPA cells, a total of 41 pathways from 1 KEGG and 40 Reactome were significantly enriched (Table 1-8): hypoxia-inducible factor (HIF) signaling pathways, which play a co-operative role in mediating the cellular response to low oxygen tension were identified in upregulated DEGs. In pathway enrichment

analyses obtained from one sample of BT-474/BPA cells compared to BT-474/Ctl (luminal B, ER+/PR+/HER2+) cells, notably, HER2 signaling pathways were identified in KEGG and Reactome pathways (data not shown).

Selection of genes and networks associated with the immune network among the DEGs of BPA-exposed MCF-7, SK-BR3, and MDA-MB-231 cells

There is substantial evidence indicating that BPA contributes to the risk of cancer by disrupting or altering the immune and inflammatory responses [2-5]. A functionally organized network of DEGs belonging to immunity and inflammation terms among MCF-7/BPA, SK-BR3/BPA and MDA-MB-231/BPA cells was created using the Cytoscape software platform. The list of significantly enriched immune-related GO terms in MCF-7/BPA, SK-BR3/BPA and MDA-MB-231/BPA cells is shown in Table 1-9.

The grouped annotation networks of immune-related GO terms among MCF-7/BPA, SK-BR3/BPA and MDA-MB-231/BPA cells are as follows: natural killer T (NKT) cell activation, CD4-positive alpha-beta cytokine production, dendritic cell migration, and regulation of natural killer cell activation (Fig. 1-4; A). Among the genes associated with the immune response, we selected HIST1H2BE, IL19, SERPINF2, IL15, CXCL5, IL12A, and CRIP1 for validation using qRT-PCR. Consistent with the RNA-seq results, the qRT-PCR results confirmed significant upregulation of IL19 (2.42-fold, p = .039) mRNA in MCF-7/BPA cells and CXCL5

(2.38-fold, p = .004) and IL12A (2.30-fold, p < .001) mRNA in SK-BR3/BPA cells and significant downregulation of IL15 (0.71-fold, p < .001) mRNA in SK-BR3/BPA cells and IL12A (0.68-fold, p = .003) and CRIP1 (0.62-fold, p = .003) expression in MDA-MB-231/BPA cells relative to the corresponding control cells (Figs. 1-4; B-D). Results of ELISA analysis indicated the similar tendency as shown in the results of RNA-seq and qRT-PCR. IL19 protein level was higher in MCF-7/BPA (1859.36 ± 207.60 pg/ml) than MCF-7 (1163.90 ± 124.0 pg/ml) (p = .028, Fig. 1-4; E). A significantly decreased IL15 protein level was observed in SK-BR3/BPA (6.21 ± 0.21 pg/ml) relative to SK-BR3 (19.21 ± 4.68 pg/ml) (p = .040). CXCL5 (18.22 ± 1.97 pg/ml) and IL12A (0.51 ± 0.07 pg/ml) in SK-BR3/BPA were significantly increased as compared with those of SK-BR3 (10.55 ± 0.63 pg/ml, and 0.18 ± 0.07 pg/ml) (p = .010 and p = .015, Fig. 1-4; F). IL12A protein was considerably lower in MDA-MB-231/BPA (0.66 ± 0.10 pg/ml) than MDA-MB-231 (1.86 ± 0.50 pg/ml) (p = .031, Fig. 1-4; G).

IL19, CA9 and SPARC upregulated by BPA are associated with poor OS in luminal a, HER-2 enriched and TN patients, respectively

We next asked whether DEGs expression identified in the different subtypes of BPA-exposed BCCs could predict the clinical outcome in breast cancer patients. The BreastMark website was used to explore the association between the expression levels of BPA-regulated DEGs and the patients'OS in luminal A, HER2-

enriched and TN subgroup. The prognostic value of top 10 up- or downregulated genes, significantly enriched GO and KEGG pathway-associated genes identified in MCF-7/BPA, SK-BR3/BPA and MDA-MB-231/BPA cells was verified by breast cancer database derived from BreastMark platform. High level of IL19 verified in MCF-7/BPA cells was associated with poor OS in luminal A subgroup (Fig. 1-5; A, n = 1163, p = .002, HR = 1.58). High level of CA9 observed in SK-BR3/BPA cells was associated with predicted poor OS in HER2-enriched subgroup (Fig. 1-5; B, n = 258, p = .013, HR = 1.646). High level of SPARC identified in MDA-MB-231/BPA cells was associated with predicted poor OS in TN subgroup (Fig. 1-5; C, n = 323, p = .006, HR = 1.714)

DISCUSSION

BPA triggers several action mechanisms, including interference with the activity of nuclear receptors such as ER as well as noncanonical steroid hormone receptors and orphan receptors [24]. The endocrine-disrupting potential of low doses of BPA, which exhibits nonmonotonic dose responses, is currently unclear. The present study is the first, to the best of our knowledge, to use transcriptome analysis approaches to demonstrate the detrimental gene signatures and biological functions regulated by chronic BPA exposure at a low dose (10^{-8} M), which was not cytotoxic, in the different subtypes of BCCs. The impacts of chronic low-dose BPA exposure on the regulation of gene expression and biological functions were dissimilar across the subtypes of BCCs.

To explore the diverse biological response of different subtypes of BCCs to BPA at concentrations relevant for human exposure, we performed RNA-seq for global gene expression profiling in MCF-7, SK-BR3 and MDA-MB-231 cells treated with 10^{-8} M BPA for 30 days. BPA can effectively substitute for estradiol in promoting growth through activation of ER-mediated signaling pathway in ER-positive breast cancer [20,25]. We here did not identify the DEGs associated with estrogenic effect in MCF-7/BPA cells. In our study, the non-estrogenic effects from BPA at low levels of exposure may be due to its relatively low affinity.

It has been reported that BPA stimulates the GPER/EGFR/ERK pathway in HER2+ cancer cells, SK-BR3 and ER-/PR-/HER2- breast cancer cells, MDA-

MB-231, mediating cancer progression [26-29]. Upregulated DEGs identified from SK-BR3/BPA cells indicated highly enriched signaling related with Rho GTPase, which is involved in EGFR pathway [30,31]. Consistent with another study [32], we observed that BPA upregulated the DEGs involved in HIF signaling pathway through GPER in MDA-MB- 231 cells.

In MCF-7/BPA cells, the top-ranked GO terms in the BP category were cellular response to gonadotropin-releasing hormone for upregulated DEGs (GPR173, MGARP) and negative regulation of fibrinolysis for downregulated DEGs (THBD, SERPINF2). Both gonadotropin-releasing hormone and its receptor are expressed by a number of malignant tumors, including those of the breast [33,34]. Gonadotropin-releasing hormone agonists, in particular goserelin, have been shown to be as therapeutically effective as surgical ovarian ablation in pre- and perimenopausal women with ER+ breast cancer [35]. The signals from gonadotropin-releasing hormone and its receptor influence the first steps of breast cancer metastasis, including proliferation, epithelial to mesenchymal transition (EMT), migration, and invasion [33]. The fibrinolytic system includes a broad spectrum of proteolytic enzymes acting in physiological and pathophysiological processes, such as hemostatic balance, tissue remodeling, tumor invasion, angiogenesis and reproduction [36]. The fibrinolysis inhibitor SERPINF2 was found at low levels in the serum of advanced breast cancer patients [37] and to restrict lymphatic remodeling and metastasis in a mouse model of cancer [38]. The expression levels of THBD (thrombomodulin) are inversely correlated with the

malignancy of BCCs [39]. This finding suggests that upregulated GPR173 and MGARP and downregulated THBD and SERPINF2 may be the detrimental gene signature pattern for developing the malignant tumors in the context of gonadotropin-releasing hormone and fibrinolysis regulation linked to BPA exposure in MCF-7 cells. Given those reports, the role of genes (GPR173, MGARP, THBD and SERPINF2) identified in MCF-7/BPA cells remains to be examined in luminal A subtype exposed to low doses of BPA.

In SK-BR3/BPA cells, the top-ranked GO terms in the BP category were cellular response to bicarbonate transport for upregulated DEGs (CA9, SLC4A8, CYB5RL) and positive regulation of inflammatory response for downregulated DEGs (PDE2A, NLRP12, IL15). There is a report that bicarbonate transporters such as the electroneutral Na+/HCO3- cotransporter (SLC4A8, NBCn1), are upregulated and play central roles in pH regulation in models of HER2+ breast cancer [40]. Based on previously published studies, chronic exposure to BPA may induce HCO3- transporter dysregulation by upregulating CA9, SLC4A8 and CYB5RL in SK-BR3 cells. The relationship between inflammation, innate immunity and cancer is accepted and suggests that inflammation is a critical component of tumor progression [41]. PDE2A is a potent antiinflammatory molecule that hydrolyses both cAMP and cGMP [42,43]. IL15 enhances innate and specific immunity, leading to tumor suppression [44,45]. Considering the fact that SK-BR3/BPA cells exhibit high expression of CA9, SLC4A8, and CYB5RL and low expression of PDE2A and IL15, the expression pattern of these genes may be a

detrimental signature associated with the dysregulation of pH, inflammation and immunity linked to BPA exposure in SK-BR3 cells. Future studies should focus on revealing the regulatory mechanisms of CA9, SLC4A8, CYB5RL, PDE2A, and IL15 expression and activity and the possible functional relevance of the changes observed in HER2-enriched subtype exposed to BPA.

In MDA-MB-231/BPA cells, the significantly enriched GO terms in the BP category were negative regulation of keratinocyte proliferation (KDF1 and EPPK1) and magnesium ion transmembrane transport (SLC41A2 and NIPAL2) for upregulated DEGs. KDF1 plays a role in the proliferation and differentiation of epidermal progenitor cells [46]. EPPK1 belongs to the plakin family of genes, which are known to function in interconnecting cytoskeletal filaments, and EPPK1 is expressed in the early stage but not in the late stages of pancreatic cancer [47]. The magnesium transporter protein SLC41A2 has potential roles in the survival or proliferation of MCF-7 cells [48]. NIPAL2, which encodes a magnesium transporter, has been suggested to be a novel tumor-promoting factor in oral squamous cell carcinoma [49]. Although the functions of KDF1, EPPK1, SLC41A2 and NIPAL2 are largely unknown in TN breast cancer, we speculate that the expression patterns of KDF1, EPPK1, SLC41A2 and NIPAL2 observed in MDA-MB-231/BPA cells may be the detrimental signatures for the transformation of epithelial cells and the formation of malignant tumors. The detailed molecular mechanism of how BPA upregulates KDF1, EPPK1, SLC41A2 and NIPAL2 and alters their normal functions should be discovered in TN subtype.

Direct exposure of ER+ BCCs to BPA, which can mimic estrogen to interact with ERα and ERβ, has been shown to be involved in multiple oncogenic signaling pathways such as MAPK, PI3K/AKT and STAT2 pathways thereby, contributing cancer development [4]. On the contrary, BPA can act via ER-independent mechanisms, which are involved in direct impact on intracellular signal transduction pathways [11]. The ER-independent mechanisms by low doses of BPA is at present still unclear. In present study, we identified the most pathways with the significant level satisfied the condition of $p < .05$, which were set to calculate the decision coefficient cut-off based on formula. Notably, the significantly enriched KEGG and PANTHER pathways linked with choline metabolism and glutamatergic synapse in upregulated DEGs were identified in MCF-7/BPA cells. Due to the casual deregulation of choline metabolism in diverse cancers, including breast cancer, abnormal choline metabolism has been considered a metabolic hallmark associated with aggressive tumor progression [50]. BPA exposure cause the elevated choline metabolism, which is underlying mechanism of highly methylated environment through the upregulation of S-adenosylmethionine (SAMe), the principal biological methyl donor involved in the choline metabolism [51]. The glutamate signaling pathway is deregulated in many cancer. Increased glutamine consumption is a hallmark of many neoplasms and cancer cells, and BCCs secreting high levels of glutamate are likely to metastasize to bone [52,53]. Activation of coagulation pathway observed in early breast cancer has been suggested to be the risk factor in a cohort of early breast cancer patients [54]. Our findings are of

notable concerns that, even under exposure to environmentally relevant doses, chronic BPA exposure can dysregulate choline metabolism and glutamate signaling pathway to support high proliferation rates and survival of luminal A BCCs.

The role of BPA in inflammatory breast cancer (IBC), which tends to be diagnosed at younger ages and is hormone receptor negative and very aggressive, has been indicated by several other studies. Recently, low dose of BPA (4×10^{-8} M), appears to aid the survival of IBC cell lines SUM149 (EGFR activated, TN) and SUM190 (ER−/PR−/HER2+) via EGFR/ERK activations and increase in SOD1 and Bcl−2 expressions, and leads to resistant to EGFR−targeted, anti−cancer drugs [17]. In our results obtained from SK−BR3 and MDA−MB−231 cells by chronic BPA exposure at 10^{-8} M, VEGF/VEGFR−mediated pathways in relation to breast cancer risk [55,56] and HIF signaling pathways, affect most of the cancer "hallmarks" including tumor metastasis and poor OS [57,58], identified in upregulated DEGs of SK−BR3/BPA and MDA−MB−231/BPA cells. The different effect of BPA on DEGs expression and biological pathways between the results obtained from IBC cell line, SUM149 and SUM190 and our results from SK−BR3 and MDA−MB−231 is probably due to the different cellular receptors as well as the dose and duration of BPA exposure. Thus, BPA may participate in a variety of different intracellular signaling pathways in a BCC subtype specific way. We suggest that the signaling pathways triggered by BPA in the BCCs of different origin should be further investigated.

The development, progression, and metastatic dissemination of cancer, as well as cancer treatment, are strongly influenced by immune and inflammatory responses [59]. BPA can use various mechanisms to modulate the immune system and affect diseases [60]. Recently, we report that chronic exposure to low-dose BPA modulates tumor inflammation mediated by macrophages, leading to the promotion of breast cancer growth and metastasis [15]. Interaction networks of NKT cell activation, T cell cytokine production, and dendritic cell migration across MCF-7/BPA, SK-BR3/BPA and MDA-MB-231/BPA cells were predicted. In this study, the significantly up- and downregulated DEGs, such as IL12A, IL15, IL19, CXCL5, and CRIP1, involved in the immune and inflammatory response in MCF-7/BPA, SK-BR3/BPA and MDA-MB-231/BPA cells were verified by qRT-PCR. Notably, IL12A, which is involved in NKT cell activation and dendritic cell migration to exert antitumor activity and antiangiogenic activity [61-63], was an overlapping DEG between SK-BR3/BPA and MDA-MB-231/BPA cells. IL12A was downregulated in MDA-MB-231/BPA cells, whereas it was upregulated in SK-BR3/BPA cells. CXCL5, which increases breast cancer progression [64], was upregulated in SK-BR3/BPA cells, while IL15, which has emerged as an immunomodulatory candidate for the treatment of cancer [44], was downregulated. IL19, which is associated with advanced tumor stage, high tumor metastasis, and worse survival in breast cancer [65], was upregulated in MCF-7/BPA cells. Low CRIP1 expression, which has been shown to be associated with an increase of BCC proliferation and invasion processes as well as a worse prognostic marker for

breast cancer patients [66], was found in MDA-MB-231/BPA cells. Taken together, these findings indicate that BPA may be a risk factor for the acceleration of breast cancer progression by regulating the expression levels of immunomodulatory genes such as IL19, CXCL5, IL12A and CRIP1 in a BCC subtype-specific manner. It is necessary to elucidate the mechanism underlying the immunomodulatory effects of BPA in breast cancer. The combination of immunotherapeutics with standard breast cancer therapies is emerging. HER2-enriched and TN breast cancers have shown evidence of immunogenicity [18,19]; thus, clinical trials are ongoing to investigate immunotherapy in combination with standard treatments. The immunomodulatory mechanism used by BPA would be helpful information for the rational design of treatments combining immunotherapy with other standard breast cancer treatments for breast cancer patients exposed to BPA.

In DEGs identified in MCF-7/BPA, SK-BR3/BPA and MDA-MB-231/BPA cells, we explored the DEGs detrimentally affected the OS of breast cancer patients classified by luminal A, HER2-enriched and TN subgroups. High expression of IL19, which plays multiple roles in immune regulation and provides a microenvironment that is conducive to tumor progression [65], detected in MCF-7/BPA cell is associated with poor OS in luminal A subtypes. CA9 identified in SK-BR3/BPA is one of the genes associated with diffusion limited hypoxia and is considered as a potential predictive marker for the both adjuvant chemotherapy- and endocrine therapy-resistant patients [67]. Our result revealed that the high

CA9 expression is detrimental gene signature to predict the poor OS in HER2-enriched subtypes. SPARC upregulated in MDA-MB-231/BPA cells belonged to the significantly enriched GO terms in the CC category (platelet alpha granule). SPARC known as osteonectin and BM40 interacts with ECM proteins to promote adhesion of cells from the matrix [68]. Increased expression of SPARC is also a poor prognostic marker for breast cancer patients [69]. In our study, high levels of SPARC is significantly associated with the poor OS of the TN breast cancer patients. We suggest that high expression of IL19, CA9, or SPARC may be the clinically relevant genes associated with detrimental impact on the OS for the luminal A, HER2-enriched, or TN breast cancer patients linked to chronic low-dose BPA exposure.

In conclusion, our results suggest that chronic BPA exposure has dissimilar impacts on the regulation of gene expression and diverse biological functions, including immune modulation, in different subtypes of BCCs. The interaction of BPA with ER is more likely to have multiple effects on the detrimental molecular mechanisms in the ER+ luminal subtype than in other subtypes. More specific studies associated with immune modulation in the HER2-enriched and TN subtypes are needed. The complex impacts of BPA should be explored in further studies to demonstrate the consequences of chronic BPA exposure in susceptible breast cancer patients and determine the relevance of the BCC subtype in terms of human BCC risk assessment.

Chapter 2

Bisphenol A Promotes the Invasive and Metastatic Potential of Ductal Carcinoma In Situ and Protumorigenic Polarization of Macrophages

INTRODUCTION

Ductal carcinoma in situ (DCIS) in the breast has been considered a seed for breast cancer [70]. Although DCIS is not life-threatening, if left untreated, 20%–50% of patients with DCIS develop invasive breast cancer within 5–10 years after initial diagnosis [71]. Little is known about what influences DCIS progression to invasive cancerous disease. The macrophages in early stage lesions have been considered major culprits in promoting the progression of premalignant DCIS to invasive breast cancer [72,73]. Based on the comparison of the effect of environmental risk factors on DCIS and invasive breast cancer, the serum estrogen level associated with the hormonal environment may act in the transformation from DCIS to invasive ductal disease [74].

Bisphenol A (BPA), a monomer used in the manufacture of polycarbonate plastics and epoxy resins, is an endocrine-disrupting environmental hormone with estrogen-like activity. BPA is able to interact with human estrogen receptors [75-77]. Although BPA has been suspected as a potential risk factor responsible for the increased incidence of breast cancer in women, most research has centered on early-life exposure to BPA in animals. These studies have linked BPA administered early and chronically at prenatal or prepubertal stages with morphological alterations in fetal mouse mammary glands [9,78-80]. There is a paucity of research on DCIS progression into invasive and metastatic breast cancer induced by BPA exposure [79,81]. The currently available data do not provide a clear role for BPA in DCIS progression into invasive breast cancer.

Many past studies have suggested that BPA has the potential to disrupt normal hormone signaling by mimicking estrogen and triggering various reproductive/endocrine and immune system disorders [82]. BPA exposure has been shown to be a dangerous risk factor for perturbation of the physiological balance of the immune system via inappropriate modulation of immune cells, leading to an increased disease risk [60,83–87]. Deleterious inflammation is observed as a primary feature of breast cancer and may initiate or enhance metastasis. Macrophages, the most abundant population in mammary tumors, are critical mediators of inflammation at each stage of breast cancer progression [88,89]. Macrophages are polarized to the classically activated M1 and the alternatively activated M2 phenotypes, which express specific M1 and M2 markers, such as nitric oxide synthase 2 (NOS2), arginase–1 (Arg–1), and CD206, and display pro– and anti–tumor immunity in breast cancer [90–92]. Very recently, a causal role for CD206+ M2 tumor–associated macrophages (TAMs) in tumor growth, as well as early dissemination and metastasis in breast cancer progression, was revealed [93,94]. BPA exposure impairs the phagocytic activity of peritoneal macrophages [95–97] and modulates TAM phenotypes [98].

The aforementioned studies provide new insight into the involvement of BPA–exposed macrophages in DCIS progression into invasive breast cancer at an early stage. However, little attention has been given to the role of BPA as a protumorigenic factor that acts through effects on TAM phenotypic regulation associated with DCIS progression. Therefore, the present study was undertaken

to investigate the effect of BPA exposure on DCIS progression to invasive and metastatic breast cancer and on the modulation of TAM phenotypes in vitro and in vivo.

MATERIALS AND METHODS

Cell lines and lentiviral transduction.

MCF10DCIS.com (ER, PR, and HER2-negative DCIS cell line) cells were purchased from Asterand (Detroit, Michigan) and were maintained in DMEM/F-12 (1:1) supplemented with 5% horse serum (HS) and 1% penicillin/streptomycin. RAW264.7 and J774A.1 cells (murine macrophages) were obtained from the Korean Cell Line Bank (Seoul, Korea) and were grown in RPMI 1640 medium (WelGENE, Daegu, Korea) containing 10% fetal bovine serum (FBS) and supplemented with a 1% antibiotic solution containing penicillin and streptomycin (ThermoFisher Scientific Inc, Waltham, Massachusetts).

A lentiviral vector containing luciferase and green fluorescence protein (GFP) constructs kindly provided by Dr Kim DE (Dongguk University Ilsan Hospital, Goyang, Korea) was used to establish Luc/GFP-transduced DCIS.com cells (DCIS.com-Luc/GFP) for the animal study. Lentiviral production and cell transduction were conducted according to the manufacturer's instructions. After lentiviral transduction, GFP-positive cells were sorted using a FACSCalibur flow cytometer (BD Biosciences, Franklin Lakes, New Jersey).

For preparation of conditioned medium (CM), DCIS.com, RAW264.7 and J774A.1 cells were cultured in a humidified incubator (37℃/5% CO_2) for 72 h, and the supernatant was collected, centrifuged at 300 × g for 5 min at 4℃, filtered

through 0.45−μm pore filters, and frozen at -80℃.

RNA−sequencing and differential gene functional annotation

For RNA preparation, DCIS.com cells were incubated with 10^{-8} M BPA or 0.1% DMSO for 30 days. Total RNA was isolated from collected cells using TRIzol reagent (Invitrogen, Carlsbad, California). RNA quality was assessed by Agilent 2100 bioanalyzer using the RNA 6000 Nano Chip (Agilent Technologies, Amstelveen, Netherlands), and RNA quantification was performed using ND−2000 Spectrophotometer (ThermoFisher Scientific Inc). Sequencing libraries were constructed using QuantSeq 3' mRNA−Seq Library Prep Kit (Lexogen, South Morang Victoria, Austria) according to the manufacturer's instructions. Highthroughput RNA−sequencing was performed as single−end 75 sequencing using NextSeq 500 system (Illumina, San Diego, California). Differentially expressed genes (DEGs) were determined based on counts from unique and multiple alignments using coverage in Bedtools [99]. The RT (Read Count) data were processed based on Quantile normalization method using EdgeR within R using Bioconductor [21]. To select DEGs, we ranked genes by the log10 p−value of genes with p−value < .05 and plotted them against the log2 fold change in a "volcano" plot. Genes upregulated and downregulated with p−value <. 05 and log ratio ≥ 1.5 were identified. To gain insight into the underlying biology of DEGs related to BPA effect, biological functional categories enriched in the DEGs were identified using the functional annotation and clustering tool of the Database for

Annotation, Visualization, and Integrated Discovery (DAVID) v6.7 (https://david.ncifcrf.gov/) [100,101]. The significant Gene Ontology (GO) terms were identified after multiple testing adjustments with the Benjamini Hochberg method were reported; Benjamini < 0.05 was considered to indicate a statistically significant difference. GO term lists (biological process [BP]; cellular compartment [CC]; molecular function [MF]) were matched with each other [102].

Cell proliferation assay

For cell proliferation assays in single culture conditions, all cells were seeded in 96-well plates at 8×10^3 cells per well and subjected to a 3-(4, 5-dimethylthiazol-2-yl)-2, 5-diphenyl tetrazolium bromide (MTT) assay. In brief, RAW264.7, J774A.1, or DCIS.com cells were incubated with 10^{-10}–10^{-4} M BPA (Sigma-Aldrich, St Louis, Missouri) for 24, 48, or 72 h. Medium was replaced with MTT-containing medium (0.25mg/ml), incubated with cells at 37℃ for 2 h, and then carefully removed. After the addition of dimethyl sulfoxide to each well, the plate was incubated at 37℃ in the dark for 5 min to solubilize formazan crystals. Absorbance was measured at 540 nm using a microplate reader (GE Healthcare, Piscataway, New Jersey). The cell viabilities are expressed as the ratio relative to untreated cells, which represent the control.

For cell proliferation assays in coculture conditions, all cells were seeded in the lower chamber of 24-well plates with a 0.4-μm pore size (BD Biosciences) at 2×10^4 cells per well and subjected to a crystal violet assay. In brief, for proliferation assays of DCIS.com cells cocultured with BPA-exposed RAW264.7

cells, 1×10^5 RAW264.7 cells were deposited in the upper chamber of a transwell plate, and 10^{-8} M BPA was added. For proliferation assays of RAW264.7 cells cocultured with BPA-exposed DCIS.com cells, 1×10^5 DCIS.com cells were deposited in the upper chamber of the transwell plate, and 10^{-8} M BPA was added. Proliferating cells were fixed in 4% paraformaldehyde and stained with crystal violet. Crystal violet from the stained lower chamber was finally extracted with 1% sodium dodecyl sulfate. The optical density at 550 nm was measured using a microplate reader (GE Healthcare), and cell proliferation was determined.

In vitro migration assays

For cell migration assays, all cells were seeded in the upper chamber of 24-well plates with a 0.8-μm pore size (BD Biosciences) at 1×10^5 cells per well and subjected to the crystal violet assay. To assess DCIS.com cell migration, DCIS.com cells were suspended in medium with 2% HS and deposited into the upper chambers. The lower chambers were filled with medium supplemented with 2% HS in the presence or absence of 10^{-8} M BPA. DCIS.com cells were incubated for 72 h at 37℃. In our coculture experiment, RAW264.7 cells were seeded into the lower chamber in the presence or absence of 10^{-8} M BPA before the migration test of DCIS.com cells.

To assess RAW264.7 cell migration, 1×10^5 cells were suspended in medium with 5% FBS and deposited into the upper chambers. The lower chambers were filled with medium supplemented with 5% FBS in the presence or absence of 10^{-8}

M BPA. RAW264.7 cells were incubated for 48 h at 37℃. In our coculture experiment, DCIS.com cells were seeded into the lower chamber in the presence or absence of 10^{-8} M BPA before the migration test of RAW264.7 cells.

The migrated cells in the bottom chamber were stained with crystal violet solution (0.5% crystal violet in 20% methanol) for 5 min. Unbound crystal violet was removed by rinsing with distilled water, and crystal violet-stained cells were subsequently air-dried. Next, crystal violet was eluted from the cells with 1% sodium dodecyl sulfate solution. The absorbance of crystal violet was measured at 550 nm using a spectrophotometer (GE Healthcare). The cell migration abilities are expressed as the ratio relative to untreated cells, which represent the control.

Quantitative real-time RT-PCR

After extraction of total RNA from cultured cells using TRIzol reagent (Invitrogen), RNA quantity and quality were determined using a NanoDrop spectrophotometer (ThermoFisher Scientific Inc). cDNA was produced using SuperScript II reverse transcriptase (Invitrogen). Real-time PCR reactions were run on an ABI 7500 system utilizing a SYBR Green PCR master mix (Applied Biosystems, Foster City, California) and specific primer sets for NOS2, Arg-1, CD206, YM-1, and FIZZ1 (Table 2-1). The results were analyzed using the ΔCt method, which reflects the threshold difference between a target gene and β-actin in each sample.

Western blotting

Cells were lysed in Radioimmunoprecipitation assay (RIPA) buffer containing a

protease inhibitor cocktail (Sigma-Aldrich), and the proteins were separated by SDS-PAGE and transferred to nitrocellulose membranes. The membranes were blocked with 5% skim milk in Tris-buffered saline and incubated with primary antibodies against phosphorylated-ERK1/2 (Cell Signaling Technology, Danvers, Massachusetts), phosphorylated-AKT (ser437) (Cell Signaling Technology), phosphorylated-FAK (Cell Signaling Technology), ERK (Cell Signaling Technology), AKT (Cell Signaling Technology), FAK (Cell Signaling Technology), NOS2 (Santa Cruz Biotechnology, Santa Cruz, California), Arg-1 (Santa Cruz Biotechnology), CD206 (Abcam, Cambridge, UK), and b-actin (Sigma-Aldrich) overnight at 4℃, followed by incubation with horseradish peroxidaseconjugated secondary antibody (Santa Cruz Biotechnology) at room temperature for an hour. The blots were developed using Enhanced Chemiluminescence Reagents (Amersham Biosciences, Piscataway, New Jersey). The relative intensity of the bands observed by Western blotting was analyzed using the ImageJ program.

Xenograft tumor model and BPA exposure conditions

Female BALB/c nude mice (3 weeks old; Orient Bio, Sungnam, Korea) were housed under a normal 12 h light/12 h dark cycle with food and water in the animal care facility of the Biomedical Research Institute of Seoul National University Hospital. Animal care and experimental procedures were performed in accordance with the Guidelines on the Ethical Use of Animals that were approved by the Institutional Animal Care and Use Committee of Seoul National University Hospital (authorization no. 16-0155-C1A0). A total of 21 female BALB/c nude mice were

used as DCIS xenograft models. For the orthotopic xenograft tumor model, 1×10^6 DCIS.com/Luc-GFP cells were resuspended in

Matrigel (BD Biosciences) and injected into the second fat pad of mice. Twenty-one mice were randomly assigned to each of 3 experimental groups: a 0.05% EtOH-control group (n = 7), a 2.5 μg/l-exposed group (n = 7), and a 25 μg/l-exposed group (n = 7). Xenograft tumor dimensions were measured using a digital caliper every 10 days, and volumes were calculated using a modified ellipsoid formula: volume = 1/2 [length $\times$ width^2], where length was defined as the largest longitudinal dimension and width as the largest transverse dimension.

According to the study reported by Jenkins et al.[12], 2.5 and 25 μg BPA (Sigma-Aldrich) was dissolved in autoclaved distilled water containing 0.05% ethanol and heated to 60℃. Mice at 3 weeks of age were exposed to 2.5 or 25 μg/l BPA via drinking water from 30 days before injection of tumor cells to post-inoculation day 40. Water with and without BPA was replaced every 3 days. As a control, ethanol was added to autoclaved distilled water at the same level present in the BPA solutions. BPA-free water bottles (Innovive, San Diego, California) were used.

Bioluminescence imaging

To monitor primary tumor growth noninvasively, bioluminescence imaging (BLI) was conducted on an IVIS luminal II system (Caliper Life Sciences, Hopkinton, Massachusetts). Every 10 days, the firefly luciferase substrate Dluciferin

(Promega, San Luis Obispo, California) was injected intraperitoneally at a dose of 150 mg/kg, and images of the tumor areas were acquired 15min later to evaluate peak intensities. The sum of all the detected photon counts within oval-shaped regions of interest was quantified in units of mean photons per second per square centimeter per steradian (p/s/cm^2/sr) using Living Image software (Caliper Life Sciences).

Histological analysis

The excised primary tumors and axillary Lymphnodes (LNs) were fixed with 4% buffered formalin and embedded in paraffin blocks. Tissues were cut into 4-μm-thick sections. Paraffin sections were deparaffinized in xylene and rehydrated in a series of graded ethanol and water solutions. For immunostaining, deparaffinized sections were immersed in 0.01 M sodium citrate buffer (pH 6.0) and blocked by incubation with 0.1 M NH_4Cl/PBS solution and 10% HS (Gibco Laboratories, Carlsbad, California) for 30 min. After incubation with primary antibodies for cytokeratin 5 (CK5) (Abcam), F4/80 (Abcam), NOS2 (Santa Cruz Biotechnology), and CD206 (Abcam), sections were incubated with HRP-conjugated secondary antibodies (Invitrogen). A Dako Liquid DAB+ Substrate Chromogen System (Agilent Technologies) was used for visualization according to the manufacturer's protocol, and hematoxylin solution (Millipore, Darmstadt, Germany) was applied for counterstaining. Histological images of stained tissues were acquired using a microscope equipped with a CCD camera (Leica, Wetzlar, Germany). Five fields at × 40 magnification within each section were randomly selected, and

immunostained cells were quantified as the percentage of brown-stained area in each microphotograph using Leica QWin image analysis and image processing software (Leica Imaging Solutions, Cambridge, UK).

Statistical analysis

The results are expressed as the mean ± standard error. Differences between groups were statistically evaluated using two-tailed t tests and ANOVA. A p-value < .05 was considered statistically significant. Statistical analyses were performed with GraphPad Prism 5.0 software (GraphPad Software, Inc, La Jolla, California).

RESULTS

Differential Gene Expression Between BPA-exposed DCIS.com Cells and Controls

The dose- or time-dependent effect of BPA on the viability and migratory ability of DCIS.com cells was determined by treatment with concentrations of BPA ranging from 10^{-10} to 10^{-4} M for 24-72 h. BPA administration resulted in a nonmonotonic response for the viability and migration of DCIS.com cells (data not shown). The viability of DCIS.com cells was significantly enhanced by BPA at a dose range of 10^{-10}-10^{-6} M but decreased at higher dose (10^{-5} and 10^{-4} M). Likewise, exposure to 10^{-8} M BPA caused a significant increase in the migration of DCIS.com cells. Therefore, we used 10^{-8} M BPA to prevent cytotoxicity. After RNA-Seq transcriptional profiling analysis of 10^{-8} M BPA-exposed DCIS.com or controls, 25737 expressed genes were identified (DRYAD DOI: doi/10.5061/dryad.770nj18). Compared with the control, 291 DEGs were identified in BPA-exposed DCIS.com cells. Of the 291 genes, 200 genes were upregulated and 91 genes were downregulated (Figs. 2-1; A and B). In top 20 enriched GO terms of BP of up- or down-regulated genes of BPA-exposed DCIS.com cells relative to control, we found GO terms such as negative regulation of cell death, cell adhesion, and immune response, namely regulation of cell proliferation and migration and immune system process (Fig. 2-1; C). Therefore, we here focused the BPA effect on the proliferative and migratory capacities of DCIS.com cells and the polarization of

macrophages to DCIS tumors.

BPA Promotes the Proliferation and Migration of DCIS.com Cells

The proliferation of DCIS.com cells treated with 10^{-8} M BPA for 24 h (1.28 ± 0.03 vs 1.00 ± 0.01, $p < .0001$), 48 h (1.74 ± 0.01 vs 1.66 ± 0.01, $p = .0008$), and 72 h (2.57 ± 0.04 vs 2.31 ± 0.03, $p = .0003$) increased in a time-dependent manner (Fig. 2-2; A). The migratory capacity of DCIS.com cells treated with 10^{-8} M BPA for 72 h (1.32 ± 0.05 vs 1.00 ± 0.05, $p = .011$) also significantly increased (Figs. 2-2; B and C). Next, the activation of intracellular molecules involved in tumor cell proliferation and migration was evaluated in BPA-treated DCIS.com cells. After cell starvation for 6 h, treatment with 10^{-8} M BPA for 15min, 30min, and 60min resulted in a significant increase in the phosphorylation levels of ERK (3.88 ± 0.57-fold, $p = .0373$; 1.74 ± 0.03-fold, $p = .0015$; 1.45 ± 0.15-fold, $p = .0897$) and FAK (1.68 ± 0.09-fold, $p = .0159$; 2.27 ± 0.29-fold, $p = .0469$; 2.24 ± 0.70-fold, $p = .2169$) but not AKT compared with untreated control cells (Figs. 2-2; D and E).

The low dose of BPA caused a significant increase in cell viability and migration in invasive breast cancer cell lines, ER-positive MCF-7 and ER-negative MDA-MB-231 cells (data not shown).

BPA Promotes the Migration Ability of RAW264.7 Cells and Upregulates the M1/M2 Phenotypic Markers NOS2, Arg-1, and

CD206

In RAW264.7 cells treated with concentrations of BPA ranging from 10^{-10} to 10^{-4} M for 24–48 h, the dose− or time−dependent effect of BPA on cell viability and migration was examined, resulting in nonmonotonic response (data not shown). Exposure to 10^{-10} to 10^{-6} M BPA did not cause significant cytotoxicity, but 10^{-5} and 10^{-4} M BPA resulted in cytotoxicity. 10^{-8} M BPA exhibited a significant and time−dependent increase in migratory ability, but 10^{-5} M BPA did not influence cell migration in RAW264.7 cell. The proliferation activity of RAW264.7 cells was not altered by exposure to 10^{-8} M BPA for 24 and 48 h (Fig. 2−3; A). An approximately 1.76− fold increase in migration was observed in RAW264.7 cells treated with 10^{-8} M BPA for 48 h (1.76 ± 0.08 vs 1.00 ± 0.07, p = .0019) (Figs. 2−3; B and C).

To explore the impact of BPA on macrophage polarization toward the M1/M2 phenotype, specific M1 (NOS2) and M2 (Arg−1, CD206, YM−1, FIZZ1) markers was examined. RAW264.7 treated with IFN−γ (20 ng/ml) plus TNF−α (20 ng/ml) for 24 h and IL−4 (50 ng/ml) plus IL−13 (20 ng/ml) for 72 h was used as M1 and M2 positive controls. A dose− and time−dependent increase in the mRNA expression of NOS2, Arg−1, and CD206 was observed in the RAW264.7 cells treated with 10^{-8} and 10^{-5} M BPA for 24 h and 4 days. Other M2 markers, YM−1 and FIZZ1 were not detected in BPA−exposed RAW264.7 cells (data not shown). Exposure to 10^{-8} M BPA for 24 h resulted in a significant increase in the levels of NOS2 (1.43 ± 0.10−fold, p = .018), Arg−1 (4.15 ± 1.03−fold, p < .0001), and

CD206 (2.11 ± 0.07−fold, p = .0007) mRNA (Fig. 2−3; D) and NOS2 (4.12 ± 1.12−fold, p = .0494), Arg−1 (4.14 ± 0.55−fold, p = .0047), and CD206 (8.10 ± 1.99−fold, p = .0233) protein (Figs. 2−3; E and F).

Additionally, BPA effect on viability, migration and M1 and M2 polarization in another macrophage cell, J774A.1 was evaluated. 10^{-8} M BPA caused a significant increase in migration as well as Arg−1 and CD206 expression in J774A.1 cells (data not shown).

BPA Augment the Migratory Ability of Both Cell Lines and the Expression of the M1/M2 Phenotypic Markers NOS2, Arg−1, and CD206 in RAW264.7 Cells Under Coculture Condition

We explored the effect of coculture with DCIS.com and RAW264.7 cells in the presence or absence of BPA on their proliferative and migratory abilities using a transwell system. The proliferation of both cells was not changed by 72 h of coculture even in the presence of 10^{-8} M BPA (Fig. 2−4; A). However, the migratory ability of DCIS.com cells was significantly increased by coculture with RAW264.7 cells (1.42 ± 0.03−fold, p< .0001) and further enhanced by coculture with BPA−exposed RAW264.7 cells (1.60 ± 0.06−fold, p< .0001), and the migratory ability of RAW264.7 cells was significantly increased by coculture with DCIS.com cells (1.41 ± 0.03−fold, p< .0001) and further enhanced by coculture with BPA−exposed DCIS.com cells (2.00 ± 0.12−fold, p< .0001) compared with

single cultures (Fig. 2−4; B).

To investigate macrophage polarization induced by communication with DCIS.com cells, M1 (NOS2) and M2 (Arg−1, CD206, YM−1, and FIZZ1) markers were examined in RAW264.7 cells treated with the DCIS.com CM or BPA−exposed DCIS.com CM. Figure 2−4; C shows a representative Western blot analysis of NOS2, Arg−1, and CD206 expression. The expression level of NOS2 was not significantly increased by DCIS.com CM (1.20 ± 0.10 vs 1.00 ± 0.00, p = .0549) but was augmented by BPA−exposed DCIS.com CM (1.51 ± 0.11 vs 1.00 ± 0.00, p = .0014) (Fig. 2−4; D). The expression levels of Arg−1 (2.09 ± 0.32, p = .0058) and CD206 (1.64 ± 0.30, p = .008) were noticeably increased by treatment with DCIS.com CM and were further enhanced by DCIS.com BPA CM (Arg−1; 2.32 ± 0.41, p = .0070 and CD206; 2.83 ± 0.30, p < .0001) (Fig. 2−4; D). However, YM−1 and FIZZ1 expression was not observed in RAW264.7 cells treated with BPA−exposed DCIS.com CM (data not shown).

We evaluated the ERα in macrophage after exposure to BPA. The ERα protein level was not increased in BPA−treated RAW264.7 cells compared with untreated RAW264.7 cells (data not shown). However, following treatment with DCIS.com CM or BPA−exposed DCIS.com CM, ERα expression was increased up to 40− to 60−fold in RAW264.7 cells treated with the DCIS.com CM (44.44 ± 8.87, p = .0072) or BPA−exposed DCIS.com CM (57.18 ± 13.77, p = .0120) relative to control cells (Figs. 2−4; E and F).

Chronic Exposure to BPA Promotes Tumor Growth in DCIS Xenograft Mice

To noninvasively monitor DCIS tumor growth, DCIS.com cells expressing both Luc and GFP were established. GFP fluorescence images and flow cytometry revealed stable GFP expression and a transduction efficiency exceeding 92% in DCIS.com/Luc−GFP cells (Figs. 2−5; A and B). Strong BLI signals ($3.90 \times 10^6 \pm 0.59$ p/s/cm^2/sr and $6.10 \times 10^6 \pm 0.06$ p/s/cm^2/sr) were detected in 8×10^3 and 1×10^4 of DCIS.com/Luc−GFP cells (Fig. 2−5; C).

In Figure 2−5; D, a schematic describing the schedule for BPA exposure and BLI monitoring in DCIS xenograft mice is presented. DCIS tumor growth was monitored using in vivo BLI and a digital caliper every 10 days post−inoculation with DCIS.com cells. Low−dose BPA exposure (2.5 μg/l) promoted DCIS tumor growth and resulted in significantly high BLI signals from tumors (23.74 ± 3.97 p/s/cm^2/sr vs 9.93 ± 1.86 p/s/cm^2/sr, $p = .0083$) at day 40 after inoculation with DCIS.com cells (Figs. 2−5; E and F). The tumor volumes (592.1 ± 87.02 mm^3 vs 361.5 ± 66.90 mm^3, $p = .0619$) at 40 days were also bigger in BPA−exposed mice than in control mice (Fig. 2−5; G). However, the body weights of mice were not different between BPA−exposed mice and control mice (Fig. 2−5; H). In high dose (25 μg/l) BPA−exposed mice, a significant increase in BLI signals and tumor volumes and weights was not observed compared with unexposed control mice (data not shown).

NOS21 TAMs Were Reduced While CD2061 TAMs Were Increased in BPA-exposed Tumor Tissues

The polarized phenotype of TAMs localized in the DCIS tumor microenvironment chronically exposed to BPA was examined in primary tumors and metastatic LNs. The gross examination and wet weight of DCIS tumors isolated from mice at post-inoculation day 40 show larger tumors with high tumor weight in the BPA-exposed group than in the control group (Figs. 2-6; A and B). A large population of TAMs evaluated by Immunohistochemistry (IHC) for F4/80 was observed at the peritumoral area of both tumors (Fig. 2-6; C). The number of TAMs positive for the M1 marker NOS2 was reduced in BPA-exposed DCIS tumors compared with control tumors (0.21 ± 0.06 vs 0.61 ± 0.11, $p = .0032$), whereas TAMs positive for the M2 marker CD206 (1.72 ± 0.17 vs 0.23 ± 0.09, $p < .0001$) were significantly increased (Figs. 2-6; C and D).

Chronic Exposure to BPA Accelerates Axillary LN Metastasis and Results in Increased CD206+ M2 TAMs

To determine the DCIS progression to invasive metastasis, the dissemination of tumor cells into axillary LNs was examined by IHC for CK5. IHC images revealed that CK5-positive tumor cells were detected in the cortex regions of LNs (Fig. 2-7; A). Quantitative analysis of IHC images revealed that the area of CK5-stained cells was significantly increased in LNs from the BPA-exposed group relative to

those from the control group (0.64 ± 0.17 vs 0.09 ± 0.05, p = .0043) (Fig. 2-7; B). BPA exposure resulted in a higher incidence of LN metastasis in mice with DCIS tumors: 10 metastatic LNs among 14 axillary LNs from the BPA-exposed group versus 3 metastatic LNs among 14 axillary LNs from the control group (Table 2-2).

The presence of NOS2+ M1 or CD206+ M2 TAMs in LNs from mice with DCIS tumors was compared with the BPA-exposed group and control group (Fig. 2-7; C). The number of NOS2+ M1 TAMs (1.17 ± 0.06) in LNs from the control group were higher than that of CD206+ M2 TAMs (0.81 ± 0.11) (p = .0086) (Fig. 2-7; D). However, BPA exposure resulted in a shift in the composition of TAM populations, with a higher number of CD206+ M2 TAMs (2.73 ± 0.54) than NOS2+ M1 TAMs (1.59 ± 0.08) and a significant increase in CD206+ M2 TAMs and a concomitant significant decrease in the NOS2+ M1 TAM population compared populations in the control group (Fig. 2-7; D).

DISCUSSION

There is still a great deal of uncertainty regarding the risk of DCIS becoming an invasive cancer in a specific patient. The carcinogenic activity of BPA is well known in estrogen-dependent breast cancer tissues and cell lines and in rodent models. However, it is not fully understood how this compound promotes invasive cancer progression from DCIS. Here, we first investigated the effects of BPA in vitro and in vivo on the regulation of DCIS cells and macrophages, which are associated with invasive breast cancer progression from DCIS.

To date, assessment of the carcinogenic potential of BPA has relied on in vitro genotoxicity assays and evaluation of peripubertal mammary glands in rodents [103]. However, the findings to date are not sufficiently strong to confirm whether BPA is truly related to DCIS progression to invasive and metastatic breast cancer. We found that 291 DEGs in BPA-exposed DCIS.com cells were enriched in GO terms of biological processing associated with cell death, proliferation, and adhesion, as well as immune response. Further studies are required to understand the functional genes differentially expressed in BPA-exposed DCIS.com cells, which may provide better insights into mechanisms underlying the BPA-associated breast cancer risk in complex DCIS progression into invasive breast cancer.

The low concentrations of BPA-exposed to adult is no more than 0.4-1.5 μg BPA/kg/day and 95% of BPA exposure does not likely exceed 1.5-4.2 μg BPA/kg/day [13]. The estimated daily intake levels of BPA in human are found in the range of 0.043-14.7 μg/kg/day and circulating levels of BPA measured from

human sera are 0.5–10 ng/ml [104]. In unintentional exposure, the circulating BPA levels in sera of elderly population and healthy nonpregnant women have been reported to be approximately 2.02–6.52 ng/ml and 1.30–8.17 ng/ml [105–107]. In the occupationally exposed population BPA levels measured from sera are approximately up to 101.94 ng/ml [108]. The dose of 20 μg/kg of BPA in female mice has been reported to be relevant to exposure in occupational workers [109]. In our study, the dose of 10^{-8} M BPA administrated in cultured cells corresponds to 2.28 ng/ml, and oral exposure of 2.5–25 μg/l BPA corresponds to 0.5–5 μg/kg/day. Based on published observations, the exposure levels of BPA chosen in this study are not much higher than that of occupationally exposed populations. Although we did not measure circulating BPA levels in sera of mice, 10^{-8} M BPA (in vitro) and 2.5 μg/l BPA (in vivo) used in our study is within a safe reference dose for humans according to the guidelines of the EPA and the U.S. Food and Drug Administration [12,14]. Hence, the dose of BPA chosen in our study is thought to be environmentally relevant and applicable to human.

BPA primarily acts by binding to classical nuclear ERs in ER–positive cancer cells. In triple negative breast cancer cells, BPA induces proliferation and migration processes via G–protein coupled estrogen receptor (GPER/GPR30) or G–protein–coupled receptor and oestrogen–related receptor c (ERRc) involved in oncogenic signaling pathways, such as PI3K/AKT–, FAK–, Src–, and ERK–dependent signal transduction pathways [17,29,110,111]. The human basal–like DCIS cell line MCF10DCIS.com, which is triple negative has been used as a model of human high–

grade comedo DCIS [112]. Based on our findings, ERK1/2− and FAK−mediated signaling pathways might be potential mechanisms for increased proliferation and migration of BPA−exposed MCF10DCIS.com cells. Nevertheless, more experimental studies are needed to further validate findings obtained from triple negative cells.

Prenatal exposure (from E9 until postnatal day 1) to BPA (2.5–25 μg/kg/day) by 50 days of age causes the formation of hyperplastic lesions and DCIS without any additional exposure to carcinogens in adulthood of rats, but there is no evidence that DCIS ultimately progresses to invasive cancer in adult mice [79,81,113]. In MMTV−erbB2 tumor mice models, chronic oral exposure of BPA (25 μg/l), but not 2500 μg BPA/L from 8 until 36 weeks of age accelerates mammary tumorigenesis and metastasis [12]. Our results show a new aspect of BPA, specifically, chronic oral exposure of DCIS xenograft mice to BPA for 70 days at an environmentally human−relevant low dose of 2.5 μg/l, but not 25 μg/l, can promote DCIS progression to metastatic breast cancer. Given that the already published data suggest an impact of BPA on the development or progression of breast cancer because of the timing and the dose, further studies focusing on the relevance of timing and dose of BPA exposure are warranted.

TAMs in peritumoral stroma have shown to be associated with a suppressive immune microenvironment and are considered powerful drivers that trigger invasion processes for breast cancer early dissemination and metastasis [93,114,115]. Much attention in recent years has been focused on the impact of

BPA on both immune-activating and immune-inhibiting processes through modulation of immune cells, including macrophages [60,82,83,85-87]. The effect of BPA on M1 and M2 macrophage polarization appears to be different in cell-type an pathologic context; BPA promotes proinflammatory M1 phenotype in mouse peritoneal macrophages, human monocytes, and macrophages cell lines THP-1 and RAW264.7 cells [83,116,117]. In contrast, BPA reduced M1 phenotypes in peritoneal macrophage [96,118,119]. In our study, although expression levels of NOS2, Arg-1, and CD206 genes are very low in BPA-treated macrophages, RAW264.7 and J774A.1 cells relative to IFN-γ plus TNF-α- or IL-4 plus IL-13-treated cells as M1 and M2 positive control, BPA elicited macrophage polarization toward a mixed M1/M2 phenotype, inducing both M1 marker (NOS2) and M2 markers (CD206, Arg-1). More importantly, BPA-exposed macrophages acquire a particular phenotype while in the tumor microenvironment, more similar to M2 phenotype than M1 phenotype. The role of ERα in the promotion of M2 macrophage activation is well known [76,120], and BPA exposure leads to infiltration of ERα-positive TAMs into the tumor microenvironment [98]. In our study, coculture with BPA-exposed DCIS.com cells or their conditioned medium remarkably augmented the expression of the M2 phenotypic markers CD206 and Arg-1 as well as that of ERα in RAW264.7 cells, suggesting that TAMs recruited to the BPA-exposed DCIS tumor microenvironment are more likely to have an M2 phenotype via ERα-mediated signaling and may exert immune-suppressive and protumorigenic activities. TAMs expressing the M2 marker CD206 are attracted

by early cancer cells from the stroma into DCIS lesions in mouse models, tend to be enriched in high-grade DCIS [121-123] and create favorable conditions for LN metastasis [94], indicating that CD206+ TAMs may function as gatekeepers to orchestrate breast cancer early dissemination and metastasis. Recently, in an ER-negative breast cancer xenograft model, a single neonatal administration of BPA promotes the growth of 4T1 cell xenografts by modulating the tumor microenvironment in the adulthood, as evidenced by higher infiltration of macrophages and lower expression of proinflammatory cytokines in the tumor microenvironment [98], implying that the observed BPA effects on tumor progression in hormone receptor-negative cancer may be primarily due to protumorigenic and suppressive immune modulation. The evidence strongly supports our findings that BPA might be a critical player in inducing protumor immune responses of CD206+M2 TAMs rather than NOS2+M1 TAMs to enhance DCIS progression to invasive breast cancer. Among the stromal cells surrounding the tumor besides the immune cells, nonimmune cells such as fibroblasts have been implicated in promoting tumor progression. The role of BPA-exposed fibroblasts in stimulating cancer progression is highlighted by Pupo et al. [124]. Future studies on BPA-exposed fibroblast are necessary to understand their role in the breast cancer progression from DCIS models. BPA displays nonmonotonic dose response characterized by low dose stimulation and high dose inhibition in diverse cells including breast cancer cells and macrophages [17,20,24,83,111,125,126]. In our study, nonmonotonic dose response of BPA was observed in DCIS.com and

RAW264.7 cells. Further studies addressing the underlying cause of the nonmonotonic dose-responses of BPA in DCIS cells and macrophages are warranted to improve the risk assessment of potential impacts of BPA on breast cancer progression.

Overall, considering the almost ubiquitous use of BPA-containing products in our daily lives, one of the most noteworthy findings of this study is that chronic BPA exposure at even an environmentally human-relevant low dose may lead to DCIS progression to invasive breast cancer through promotion of DCIS.com cell proliferation and migration and the protumorigenic polarization phenotype of TAMs. DCIS may develop faster and is more likely to progress to invasive and metastatic breast cancer among populations environmentally and occupationally exposed to BPA. We suggest that BPA concentrations and immune responses in the tissues and organs of patients diagnosed with DCIS and exposed to BPA need to be carefully analyzed.

TABLES

Table 1-1. Specific primer sequences used for real-time RT-PCR (Ⅰ).

Gene		Sequence (5′ −>3′)
HIST1H2BE	Forward	CCTGGCGCATTACAACAAGC
	Reverse	TACTAAGGCAGTTGCAGGGA
IL19	Forward	CTACGTGGACAGGGTGTTCAA
	Reverse	GATGACTCTGGTGGCATTGGT
SERPINF2	Forward	TTCTCCTCAACGCCATCCAC
	Reverse	AAGGGGAAATGAGCCACCTG
IL15	Forward	CATTTTGGGCTGTTTCAGTGC
	Reverse	TGGGGTGAACATCACTTTCCG
CXCL5	Forward	GTTGAGAGAGCTGCGTTGC
	Reverse	TTGGAGCACTGTGGGCCTAT
IL12A	Forward	TACCCTTGCACTTCTGAAGAGATT
	Reverse	GCCAGGCAACTCCCATTAGTT
CRIP1	Forward	GTGTCCCAAGTGCAACAAGG
	Reverse	GGTCAGCGTCTTCCCACATT
β -actin	Forward	TTCCTGGGCATGGAGTCCTGTGG
	Reverse	CGCCTAGAAGCATTTGCGGTGG

Table 1-2. Top 10 up- or downregulated genes ordered by p-value and fold change in MCF-7/BPA cells.

	NCBI ID	HUGO	Gene Name	P-value	Fold change
Upregulated genes	9481	SLC25A27	solute carrier family 25 member 27	6.E-03	5.707
	6855	SYP	synaptophysin	4.E-02	4.784
	101927217	LINC01473	long intergenic non-protein coding RNA 1473	1.E-02	4.551
	353500	BMP8A	bone morphogenetic protein 8a	1.E-02	4.067
	199223	TTC21A	tetratricopeptide repeat domain 21A	3.E-02	4.065
	100507257	MEG9	maternally expressed 9 (non-protein coding)	3.E-02	3.875
	83888	FGFBP2	fibroblast growth factor binding protein 2	3.E-03	3.617
	6505	SLC1A1	solute carrier family 1 member 1	2.E-02	3.464
	684959	SNORA25	small nucleolar RNA, H/ACA box 25	3.E-02	3.323
	126969	SLC44A3	solute carrier family 44 member 3	2.E-02	3.313
Downregulated genes	101928272	LOC101928272	uncharacterized LOC101928272	4.E-02	0.174
	2348	FOLR1	folate receptor 1 (adult)	2.E-02	0.225
	400046	FLJ41278	uncharacterized LOC400046	5.E-03	0.253
	794	CALB2	calbindin 2	4.E-02	0.255
	403323	LOC403323	uncharacterized LOC403323	8.E-03	0.265

	347	APOD	apolipoprotein D	2.E-02	0.277
	115827	RAB3C	RAB3C, member RAS oncogene family	3.E-02	0.284
	4675	NAP1L3	nucleosome assembly protein 1 like 3	1.E-03	0.301
	199221	DZIP1L	DAZ interacting zinc finger protein 1 like	6.E-03	0.317
	2634	GBP2	guanylate binding protein 2	4.E-02	0.318

Table 1-3. Top 10 up- or downregulated genes ordered by p-value and fold change in SK-BR3/BPA cells.

	NCBI ID	HUGO	Gene Name	P-value	Fold change
Upregulated genes	100507582	BHLHE40-AS1	BHLHE40 antisense RNA 1	6.E-03	4.960
	112714	TUBA3E	tubulin alpha 3e	5.E-02	4.388
	83592	AKR1E2	aldo-keto reductase family 1, member E2	2.E-03	4.296
	339942	H1FX-AS1	H1FX antisense RNA 1	4.E-03	4.264
	55466	DNAJA4	DnaJ heat shock protein family (Hsp40) member A4	2.E-02	4.227
	101928402	LOC101928402	uncharacterized LOC101928402	2.E-03	3.836
	100750225	PCAT1	prostate cancer associated transcript 1 (non-protein coding)	6.E-04	3.800
	340267	COL28A1	collagen type XXVIII alpha 1	4.E-02	3.593
	728463	TGFB2-AS1	TGFB2 antisense RNA 1 (head to head)	3.E-02	3.566
	339983	NAT8L	N-acetyltransferase 8 like	1.E-03	3.562
Downregulated genes	56936	CCDC177	coiled-coil domain containing 177	2.E-02	0.117
	66037	BOLL	boule homolog, RNA binding protein	5.E-02	0.177
	11245	GPR176	G protein-coupled receptor 176	1.E-02	0.177
	114757	CYGB	cytoglobin	3.E-02	0.212
	219736	STOX1	storkhead box 1	4.E-02	0.225

	5138	PDE2A	phosphodiesterase 2A	3.E-02	0.248
	26774	SNORD80	small nucleolar RNA, C/D box 80	3.E-02	0.265
	387849	REP15	RAB15 effector protein	2.E-02	0.266
	123041	SLC24A4	solute carrier family 24 member 4	9.E-03	0.275
	339488	TFAP2E	transcription factor AP-2 epsilon	9.E-03	0.293

Table 1-4. Top 10 up- or downregulated genes ordered by p-value and fold change in MDA-MB-231/BPA cells.

	NCBI ID	HUGO	Gene Name	P-value	Fold change
Upregulated genes	387700	SLC16A12	solute carrier family 16 member 12	4.E-02	4.679
	83481	EPPK1	epiplakin 1	2.E-03	4.342
	27443	CECR2	cat eye syndrome chromosome region, candidate 2	2.E-02	3.906
	100130889	PSORS1C3	psoriasis susceptibility 1 candidate 3 (non-protein coding)	1.E-03	3.649
	54979	HRASLS2	HRAS like suppressor 2	8.E-03	3.373
	9023	CH25H	cholesterol 25-hydroxylase	2.E-02	3.330
	100129583	FAM47E	family with sequence similarity 47 member E	1.E-03	3.214
	56624	ASAH2	N-acylsphingosine amidohydrolase (non-lysosomal ceramidase) 2	3.E-02	3.109
	4166	CHST6	carbohydrate sulfotransferase 6	4.E-02	3.107
	126695	KDF1	keratinocyte differentiation factor 1	4.E-02	2.731
Downregulated genes	677819	SNORA37	small nucleolar RNA, H/ACA box 37	2.E-03	0.173
	27033	ZBTB32	zinc finger and BTB domain containing 32	4.E-02	0.270
	283692	CPEB1-AS1	CPEB1 antisense RNA 1	8.E-03	0.270
	283102	KRT8P41	keratin 8 pseudogene 41	3.E-02	0.276

	91544	UBXN11	UBX domain protein 11	3.E-02	0.282
	81698	LINC00597	long intergenic non-protein coding RNA 597	1.E-02	0.289
	163589	TDRD5	tudor domain containing 5	4.E-02	0.298
	283392	TRHDE-AS1	TRHDE antisense RNA 1	1.E-02	0.300
	100133315	LOC100133315	transient receptor potential cation channel, subfamily C, member 2-like	1.E-02	0.311
	26782	SNORA66	small nucleolar RNA, H/ACA box 66	2.E-02	0.317

Table 1-5. List of significantly enriched GO terms and genes in MCF-7/BPA, SK-BR3/BPA, and MDA-MB-231/BPA cells using the DAVID tool.

Cell lines	GO terms	NCBI ID	HUGO	Gene Name	P-value	Fold change
MCF-7 /BPA	[BP] cellular response to gonadotropin-releasing hormone (GO:0097211)	54328	GPR173	G protein-coupled receptor 173	2.E-02	2.248
		84709	MGARP	mitochondria localized glutamic acid rich protein	2.E-04	2.657
	[BP] regulation of transcription, DNA-templated (GO:0006355)	10656	KHDRBS3	KH domain containing, RNA binding, signal transduction associated 3	4.E-02	3.244
		9310	ZNF235	zinc finger protein 235	4.E-02	2.218
		126068	ZNF441	zinc finger protein 441	4.E-02	1.734
		7068	THRB	thyroid hormone receptor beta	9.E-03	1.557
		100129842	ZNF737	zinc finger protein 737	2.E-03	1.508
		126069	ZNF491	zinc finger protein 491	5.E-02	2.557
		6473	SHOX	short stature homeobox	5.E-02	2.479
		5079	PAX5	paired box 5	5.E-02	1.700
		4303	FOXO4	forkhead box O4	1.E-02	1.766
		10661	KLF1	Kruppel-like factor 1 (erythroid)	1.E-02	1.820
	[BP]intraciliary retrograde transport (GO:0035721)	57728	WDR19	WD repeat domain 19	1.E-02	1.703
		199223	TTC21A	tetratricopeptide repeat domain 21A	3.E-02	4.065
	[BP]chemical synaptic transmission (GO:0007268)	2913	GRM3	glutamate metabotropic receptor 3	4.E-02	2.228
		2905	GRIN2C	glutamate ionotropic receptor NMDA type subunit 2C	9.E-03	1.698
		3352	HTR1D	5-hydroxytryptamine receptor 1D	4.E-02	1.603

		6505	SLC1A1	solute carrier family 1 member 1	2.E-02	3.464
	[BP] brain development (GO:0007420)	347	APOD	apolipoprotein D	2.E-02	0.277
		6770	STAR	steroidogenic acute regulatory protein	2.E-02	0.474
		4435	CITED1	Cbp/p300 interacting transactivator with Glu/Asp rich carboxy-terminal domain 1	4.E-02	0.347
	[BP] negative regulation of fibrinolysis (GO:0051918)	7056	THBD	thrombomodulin	2.E-02	0.645
		5345	SERPINF2	serpin family F member 2	3.E-02	0.368
	[CC] intraciliary transport particle A (GO:0030991)	57728	WDR19	WD repeat domain 19	1.E-02	1.703
		199223	TTC21A	tetratricopeptide repeat domain 21A	3.E-02	4.065
	[MF] lipid transporter activity (GO:0005319)	10877	CFHR4	complement factor H related 4	1.E-02	0.483
		347	APOD	apolipoprotein D	2.E-02	0.277
SK-BR3 /BPA	[BP] bicarbonate transport (GO:0015701)	768	CA9	carbonic anhydrase 9	4.E-02	3.430
		9498	SLC4A8	solute carrier family 4 member 8	4.E-02	2.469
		606495	CYB5RL	cytochrome b5 reductase like	0.014	2.074
	[BP] definitive hemopoiesis (GO:0060216)	3213	HOXB3	homeobox B3	1.E-03	2.141
		8076	MFAP5	microfibrillar associated protein 5	4.E-02	1.968
	[BP] positive regulation of inflammatory response (GO:0050729)	5138	PDE2A	phosphodiesterase 2A	3.E-02	0.248
		91662	NLRP12	NLR family, pyrin domain containing 12	9.E-04	0.456
		3600	IL15	interleukin 15	4.E-03	0.404
		5138	PDE2A	phosphodiesterase 2A	3.E-02	0.248
		123041	SLC24A4	solute carrier family 24 member 4	9.E-03	0.275

	[BP]calcium ion transmembrane transport (GO:0070588)	2903	GRIN2A	glutamate ionotropic receptor NMDA type subunit 2A	1.E-02	0.406
	[BP] superoxide anion generation (GO:0042554)	79400	NOX5	NADPH oxidase, EF-hand calcium binding domain 5	4.E-02	0.397
		4688	NCF2	neutrophil cytosolic factor 2	5.E-02	0.449
	[BP] signal transduction (GO:0007165)	343578	ARHGAP40	Rho GTPase activating protein 40	4.E-02	0.550
		5138	PDE2A	phosphodiesterase 2A	3.E-02	0.248
		2796	GNRH1	gonadotropin releasing hormone 1	3.E-02	0.324
		91662	NLRP12	NLR family, pyrin domain containing 12	9.E-04	0.456
		1139	CHRNA7	cholinergic receptor nicotinic alpha 7 subunit	4.E-02	0.397
		3600	IL15	interleukin 15	4.E-03	0.404
		27329	ANGPTL3	angiopoietin like 3	3.E-03	0.395
	[CC] extracellular region (GO:0005576)	7424	VEGFC	vascular endothelial growth factor C	3.E-03	3.175
		6374	CXCL5	C-X-C motif chemokine ligand 5	4.E-03	2.843
		57758	SCUBE2	signal peptide, CUB domain and EGF like domain containing 2	9.E-03	2.506
		64109	CRLF2	cytokine receptor-like factor 2	9.E-03	2.488
		3592	IL12A	interleukin 12A	4.E-02	1.795
		340267	COL28A1	collagen type XXVIII alpha 1	4.E-02	3.593
		140881	DEFB129	defensin beta 129	4.E-02	3.263
		8076	MFAP5	microfibrillar associated protein 5	4.E-02	1.968
		8620	NPFF	neuropeptide FF-amide peptide precursor	5.E-03	3.180
		5552	SRGN	serglycin	6.E-03	1.872
	[CC] integral component of	11245	GPR176	G protein-coupled receptor 176	1.E-02	0.177
		123041	SLC24A4	solute carrier family 24 member 4	9.E-03	0.275

	plasma membrane (GO:0005887)	388630	TRABD2B	TraB domain containing 2B	3.E-02	0.350
		2903	GRIN2A	glutamate ionotropic receptor NMDA type subunit 2A	1.E-02	0.406
		3600	IL15	interleukin 15	4.E-03	0.404
		8170	SLC14A2	solute carrier family 14 member 2	3.E-02	0.320
	[MF] calcium channel activity (GO:0005262)	5138	PDE2A	phosphodiesterase 2A	3.E-02	0.248
		123041	SLC24A4	solute carrier family 24 member 4	9.E-03	0.275
		2903	GRIN2A	glutamate ionotropic receptor NMDA type subunit 2A	1.E-02	0.406
	[MF] superoxide-generating NADPH oxidase activity (GO:0016175)	79400	NOX5	NADPH oxidase, EF-hand calcium binding domain 5	4.E-02	0.397
		4688	NCF2	neutrophil cytosolic factor 2	5.E-02	0.449
	[MF] protein homodimerization activity (GO:0042803)	5138	PDE2A	phosphodiesterase 2A	3.E-02	0.248
		1139	CHRNA7	cholinergic receptor nicotinic alpha 7 subunit	4.E-02	0.397
		284359	IZUMO1	izumo sperm-egg fusion 1	3.E-02	0.377
		169026	SLC30A8	solute carrier family 30 member 8	7.E-03	0.416
		339488	TFAP2E	transcription factor AP-2 epsilon	9.E-03	0.293
MDA-MB-231/BPA	[BP] negative regulation of keratinocyte proliferation (GO:0010839)	126695	KDF1	keratinocyte differentiation factor 1	4.E-02	2.731
		83481	EPPK1	epiplakin 1	2.E-03	4.342
	[BP] magnesium ion transmembrane transport (GO:1903830)	84102	SLC41A2	solute carrier family 41 member 2	2.E-02	1.508
		79815	NIPAL2	NIPA like domain containing 2	3.E-02	1.611

	[CC] platelet alpha granule (GO:0031091)	6678	SPARC	secreted protein acidic and cysteine rich	2.E-02	2.320
		7058	THBS2	thrombospondin 2	1.E-02	2.665
	[MF] magnesium ion transmembrane transporter activity (GO:0015095)	84102	SLC41A2	solute carrier family 41 member 2	2.E-02	1.508
		79815	NIPAL2	NIPA like domain containing 2	3.E-02	1.611

BP: biological process, CC: cellular component, MF: molecular function

Table 1-6. The significantly enriched pathways of the DEGs in MCF-7/BPA cells.

	Pathway database	Term	Pathway	P-value
Upregulated DEGs	KEGG pathways	hsa04724	Glutamatergic synapse	5.00E-03
		hsa05231	Choline metabolism in cancer	4.00E-02
	PANTHER pathways	P02778	Sulfate assimilation	1.05E-02
		P02740	De novo pyrimidine ribonucleotides biosynthesis	4.81E-02
		P00037	Ionotropic glutamate receptor pathway	8.12E-04
		P00039	Metabotropic glutamate receptor group III pathway	2.52E-02
	Reactome pathways	R-HSA-5619067	Defective SLC1A1 is implicated in schizophrenia 18 (SCZD18) and dicarboxylic aminoaciduria (DCBXA)	7.01E-03
		R-HSA-3560796	Defective PAPSS2 causes SEMD-PA	7.01E-03
		R-HSA-111995	phospho-PLA2 pathway	1.05E-02
		R-HSA-2408550	Metabolism of ingested H2SeO4 and H2SeO3 into H2Se	1.40E-02
		R-HSA-8849468	PTK6 Regulates Proteins Involved in RNA Processing	2.09E-02
		R-HSA-166187	Mitochondrial Uncoupling Proteins	2.09E-02
		R-HSA-167827	The proton buffering model	2.09E-02
		R-HSA-167826	The fatty acid cycling model	2.09E-02
		R-HSA-1482798	Acyl chain remodeling of CL	2.43E-02
		R-HSA-8939245	RUNX1 regulates transcription of genes involved in BCR	2.43E-02

	signaling	
R-HSA-174362	Transport and synthesis of PAPS	2.43E-02
R-HSA-196843	Vitamin B2 (riboflavin) metabolism	2.78E-02
R-HSA-418886	Netrin mediated repulsion signals	3.12E-02
R-HSA-3656244	Defective B4GALT1 causes B4GALT1-CDG (CDG-2d)	3.12E-02
R-HSA-3656243	Defective ST3GAL3 causes MCT12 and EIEE15	3.12E-02
R-HSA-3656225	Defective CHST6 causes MCDC1	3.12E-02
R-HSA-190377	FGFR2b ligand binding and activation	3.46E-02
R-HSA-427601	Multifunctional anion exchangers	3.46E-02
R-HSA-159763	Transport of gamma-carboxylated protein precursors from the endoplasmic reticulum to the Golgi apparatus	3.46E-02
R-HSA-1483115	Hydrolysis of LPC	3.46E-02
R-HSA-549127	Organic cation transport	3.80E-02
R-HSA-159782	Removal of aminoterminal propeptides from gamma-carboxylated proteins	3.80E-02
R-HSA-418889	via Dependence Receptors in the absence of ligand	3.80E-02
R-HSA-159740	Gamma-carboxylation of protein precursors	3.80E-02
R-HSA-376172	DSCAM interactions	4.14E-02
R-HSA-159854	Gamma-carboxylation, transport, and amino-terminal cleavage of proteins	4.14E-02

		R-HSA-446107	Type I hemidesmosome assembly	4.14E-02
		R-HSA-390666	Serotonin receptors	4.47E-02
		R-HSA-2022857	Keratan sulfate degradation	4.81E-02
		R-HSA-3560782	Diseases associated with glycosaminoglycan metabolism	1.00E-02
		R-HSA-373752	Netrin-1 signaling	1.39E-02
		R-HSA-111885	Opioid Signalling	3.45E-02
		R-HSA-425366	Transport of bile salts and organic acids, metal ions and amine compounds	3.84E-02
		R-HSA-425407	SLC-mediated transmembrane transport	1.12E-02
		R-HSA-5673001	RAF/MAP kinase cascade	4.88E-02
		R-HSA-418594	G alpha (i) signalling events	1.29E-02
Downregulated DEGs	KEGG pathways	hsa04610	Complement and coagulation cascades	1.E-02
		hsa0532:	Systemic lupus erythematosus	4.E-02
	PANTHER pathways	P02751	Lysine biosynthesis	5.88E-03
		P00011	Blood coagulation	8.82E-03
	Reactome pathways	R-HSA-8942233	Intestinal infectious diseases	8.81E-03
		R-HSA-211994	Sterols are 12-hydroxylated by CYP8B1	8.81E-03
		R-HSA-964827	Progressive trimming of alpha-1,2-linked mannose residues from Man9/8/7GlcNAc2 to produce Man5GlcNAc2	1.17E-02

R-HSA-196836	Vitamin C (ascorbate) metabolism	3.78E-04
R-HSA-964739	N-glycan trimming and elongation in the cis-Golgi	1.75E-02
R-HSA-1566977	Fibronectin matrix formation	2.04E-02
R-HSA-174577	Activation of C3 and C5	2.33E-02
R-HSA-8941332	RUNX2 regulates genes involved in cell migration	2.33E-02
R-HSA-804914	Transport of fatty acids	2.62E-02
R-HSA-390247	Beta-oxidation of very long chain fatty acids	2.62E-02
R-HSA-5362798	Release of Hh-Np from the secreting cell	2.62E-02
R-HSA-211999	CYP2E1 reactions	3.48E-02
R-HSA-8866907	Activation of the TFAP2 (AP-2) family of transcription factors	3.76E-02
R-HSA-196108	Pregnenolone biosynthesis	3.76E-02
R-HSA-211979	Eicosanoids	3.76E-02
R-HSA-211958	Miscellaneous substrates	3.76E-02
R-HSA-75205	Dissolution of Fibrin Clot	4.05E-02
R-HSA-5357786	TNFR1-induced proapoptotic signaling	4.05E-02
R-HSA-3656253	Defective EXT1 causes exostoses 1, TRPS2 and CHDS	4.33E-02
R-HSA-3656237	Defective EXT2 causes exostoses 2	4.33E-02
R-HSA-193775	Synthesis of bile acids and bile salts via 24-hydroxycholesterol	4.33E-02

	R-HSA-193807	Synthesis of bile acids and bile salts via 27-hydroxycholesterol	4.61E-02
	R-HSA-2162123	Synthesis of Prostaglandins (PG) and Thromboxanes (TX)	4.61E-02
	R-HSA-5676594	TNF receptor superfamily (TNFSF) members mediating non-canonical NF-kB pathway	4.89E-02
	R-HSA-211897	Cytochrome P450 - arranged by substrate type	1.67E-02
	R-HSA-8873719	RAB geranylgeranylation	1.67E-02
	R-HSA-196849	Metabolism of water-soluble vitamins and cofactors	5.72E-03
	R-HSA-196854	Metabolism of vitamins and cofactors	2.38E-03
	R-HSA-211945	Phase I - Functionalization of compounds	3.97E-02
	R-HSA-977606	Regulation of Complement cascade	4.31E-02
	R-HSA-8942233	Intestinal infectious diseases	8.81E-03

Table 1-7. The significantly enriched pathways of the DEGs in SK-BR3/BPA cells.

	Pathway database	Term	Pathway	P-value
Upregulated DEGs	Reactome pathways	R-HSA-194313	VEGF ligand-receptor interactions	3.78E-04
		R-HSA-194306	Neurophilin interactions with VEGF and VEGFR	1.46E-02
		R-HSA-195399	VEGF binds to VEGFR leading to receptor dimerization	3.78E-04
		R-HSA-5362798	Release of Hh-Np from the secreting cell	2.62E-02
		R-HSA-389397	Orexin and neuropeptides FF and QRFP bind to their respective receptors	2.62E-02
		R-HSA-1296052	Ca2+ activated K+ channels	2.91E-02
		R-HSA-190840	Microtubule-dependent trafficking of connexons from Golgi to the plasma membrane	1.73E-03
		R-HSA-425381	Bicarbonate transporters	3.19E-02
		R-HSA-190872	Transport of connexons to the plasma membrane	1.90E-03
		R-HSA-1234158	Regulation of gene expression by Hypoxia-inducible Factor	3.48E-02
		R-HSA-389977	Post-chaperonin tubulin folding pathway	2.26E-03
		R-HSA-1480926	O2/CO2 exchange in erythrocytes	3.76E-02
		R-HSA-1475029	Reversible hydration of carbon dioxide	3.76E-02
		R-HSA-1237044	Erythrocytes take up carbon dioxide and release oxygen	3.76E-02

R-HSA-8984722	Interleukin-35 Signalling	3.76E-02
R-HSA-389960	Formation of tubulin folding intermediates by CCT/TriC	2.86E-03
R-HSA-5626467	RHO GTPases activate IQGAPs	4.25E-03
R-HSA-389958	Cooperation of Prefoldin and TriC/CCT in actin and tubulin folding	4.50E-03
R-HSA-190861	Gap junction assembly	5.89E-03
R-HSA-3371497	HSP90 chaperone cycle for steroid hormone receptors (SHR)	7.03E-04
R-HSA-8955332	Carboxyterminal post-translational modifications of tubulin	7.45E-03
R-HSA-437239	Recycling pathway of L1	9.18E-03
R-HSA-190828	Gap junction trafficking	9.54E-03
R-HSA-157858	Gap junction trafficking and regulation	9.91E-03
R-HSA-6811436	COPI-independent Golgi-to-ER retrograde traffic	1.11E-02
R-HSA-983189	Kinesins	1.48E-02
R-HSA-194138	Signaling by VEGF	3.88E-03
R-HSA-1445148	Translocation of SLC2A4 (GLUT4) to the plasma membrane	1.96E-02
R-HSA-8852276	The role of GTSE1 in G2/M progression after G2 checkpoint	2.33E-02
R-HSA-380320	Recruitment of NuMA to mitotic centrosomes	3.20E-02

		R-HSA-390466	Chaperonin-mediated protein folding	3.26E-02
		R-HSA-6811434	COPI-dependent Golgi-to-ER retrograde traffic	3.64E-02
		R-HSA-391251	Protein folding	3.64E-02
		R-HSA-6807878	COPI-mediated anterograde transport	3.70E-02
		R-HSA-425393	Transport of inorganic cations/anions and amino acids/oligopeptides	3.97E-02
		R-HSA-373760	L1CAM interactions	4.88E-02
		R-HSA-375276	Peptide ligand-binding receptors	1.83E-02
		R-HSA-195258	RHO GTPase Effectors	5.00E-02
		R-HSA-2262752	Cellular responses to stress	2.95E-02
		R-HSA-109582	Hemostasis	4.86E-02
Downregulated DEGs	Reactome pathways	R-HSA-5619055	Defective SLC24A4 causes hypomineralized amelogenesis imperfecta (AI)	4.56E-03
		R-HSA-8981607	Intracellular oxygen transport	9.09E-03
		R-HSA-1300652	Sperm:Oocyte Membrane Binding	1.36E-02
		R-HSA-435368	Zinc efflux and compartmentalization by the SLC30 family	1.81E-02
		R-HSA-1236973	Cross-presentation of particulate exogenous antigens (phagosomes)	2.03E-02
		R-HSA-8866904	Negative regulation of activity of TFAP2 (AP-2) family transcription factors	2.48E-02

	R-HSA-629594	Highly calcium permeable postsynaptic nicotinic acetylcholine receptors	2.70E-02
	R-HSA-203615	eNOS activation	2.70E-02
	R-HSA-425561	Sodium/Calcium exchangers	2.70E-02
	R-HSA-8866907	Activation of the TFAP2 (AP-2) family of transcription factors	2.93E-02
	R-HSA-375281	Hormone ligand-binding receptors	3.15E-02
	R-HSA-5668599	RHO GTPases Activate NADPH Oxidases	3.15E-02
	R-HSA-8983432	Interleukin-15 signaling	3.37E-02
	R-HSA-622327	Postsynaptic nicotinic acetylcholine receptors	3.37E-02
	R-HSA-181431	Acetylcholine binding and downstream events	3.37E-02
	R-HSA-629602	Activation of Nicotinic Acetylcholine Receptors	3.37E-02
	R-HSA-202131	Metabolism of nitric oxide	3.59E-02
	R-HSA-203765	eNOS activation and regulation	3.59E-02
	R-HSA-442729	CREB phosphorylation through the activation of CaMKII	3.59E-02
	R-HSA-442982	Ras activation upon Ca2+ influx through NMDA receptor	4.03E-02
	R-HSA-438066	Unblocking of NMDA receptor, glutamate binding and activation	4.03E-02
	R-HSA-435354	Zinc transporters	4.03E-02

	R-HSA-418457	cGMP effects	4.03E-02
	R-HSA-3299685	Detoxification of Reactive Oxygen Species	3.22E-03
	R-HSA-8963889	Assembly of active LPL and LIPC lipase complexes	4.25E-02
	R-HSA-8849932	Synaptic adhesion-like molecules	4.90E-02
	R-HSA-425366	Transport of bile salts and organic acids, metal ions and amine compounds	1.72E-02
	R-HSA-112314	Neurotransmitter receptors and postsynaptic signal transmission	4.60E-02
	R-HSA-425407	SLC-mediated transmembrane transport	1.85E-02
	R-HSA-382551	Transport of small molecules	2.37E-02

Table 1-8. The significantly enriched pathways of the DEGs in MDA-MB-231/BPA cells.

	Pathway database	Term	Pathway	P-value
Upregulated DEGs	PANTHER pathways	P00050	Plasminogen activating cascade	3.09E-02
	Reactome pathways	R-HSA-1234162	Oxygen-dependent asparagine hydroxylation of Hypoxia-inducible Factor Alpha	6.26E-03
		R-HSA-3000497	Scavenging by Class H Receptors	7.82E-03
		R-HSA-8849473	PTK6 Expression	9.38E-03
		R-HSA-3656225	Defective CHST6 causes MCDC1	1.40E-02
		R-HSA-5602498	MyD88 deficiency (TLR2/4)	1.71E-02
		R-HSA-1234158	Regulation of gene expression by Hypoxia-inducible Factor	1.87E-02
		R-HSA-5603041	IRAK4 deficiency (TLR2/4)	1.87E-02
		R-HSA-75205	Dissolution of Fibrin Clot	2.18E-02
		R-HSA-5686938	Regulation of TLR by endogenous ligand	3.09E-02
		R-HSA-5260271	Diseases of Immune System	3.85E-02
		R-HSA-180024	DARPP-32 events	3.85E-02
		R-HSA-5602358	Diseases associated with the TLR signaling cascade	3.85E-02
		R-HSA-425410	Metal ion SLC transporters	4.15E-02

		R-HSA-5223345	Miscellaneous transport and binding events	4.15E-02
		R-HSA-2022854	Keratan sulfate biosynthesis	4.46E-02
		R-HSA-1482839	Acyl chain remodelling of PE	4.61E-02
		R-HSA-2022928	HS-GAG biosynthesis	4.90E-02
		R-HSA-1630316	Glycosaminoglycan metabolism	1.64E-02
		R-HSA-114608	Platelet degranulation	1.74E-02
		R-HSA-76005	Response to elevated platelet cytosolic Ca2+	1.87E-02
		R-HSA-3781865	Diseases of glycosylation	2.11E-02
Downregulated DEGs	Reactome pathways	R-HSA-5683177	Defective ABCC8 can cause hypoglycemias and hyperglycemias	7.25E-03
		R-HSA-1296025	ATP sensitive Potassium channels	1.21E-02
		R-HSA-380095	Tachykinin receptors bind tachykinins	1.45E-02
		R-HSA-428543	Inactivation of CDC42 and RAC1	2.16E-02
		R-HSA-8851805	MET activates RAS signaling	2.40E-02
		R-HSA-203615	eNOS activation	2.87E-02
		R-HSA-211999	CYP2E1 reactions	2.87E-02
		R-HSA-264870	Caspase-mediated cleavage of cytoskeletal proteins	3.11E-02
		R-HSA-8984722	Interleukin-35 Signalling	3.11E-02
		R-HSA-211958	Miscellaneous substrates	3.11E-02

	R-HSA-202131	Metabolism of nitric oxide	3.81E-02
	R-HSA-203765	eNOS activation and regulation	3.81E-02
	R-HSA-199220	Vitamin B5 (pantothenate) metabolism	4.27E-02
	R-HSA-1912420	Pre-NOTCH Processing in Golgi	4.51E-02
	R-HSA-5083636	Defective GALNT12 causes colorectal cancer 1 (CRCS1)	4.74E-02
	R-HSA-5083632	Defective C1GALT1C1 causes Tn polyagglutination syndrome (TNPS)	4.74E-02
	R-HSA-5083625	Defective GALNT3 causes familial hyperphosphatemic tumoral calcinosis (HFTC)	4.74E-02
	R-HSA-5423646	Aflatoxin activation and detoxification	4.97E-02
	R-HSA-2672351	Stimuli-sensing channels	2.83E-02

Table 1-9. List of significantly enriched GO terms associated with the immune network in MCF-7/BPA, SK-BR3/BPA, and MDA-231/BPA cells using the Cytoscape tool.

Cell	Immune GO Term	P-value
MCF-7/BPA	NKT cell activation	0.01
	Dendritic cell migration	0.04
SK-BR3/BPA	CD4-positive, alpha-beta T cell cytokine production	0.03
MDA-MB-231/BPA	Positive regulation of natural killer cell activation	0.02
	Regulation of natural killer cell activation	0.04
SK-BR3/BPA	T-helper 1 cell activation	0.04
	Toll-like receptor 1 signaling pathway	0.01
MDA-MB-231/BPA	Extrathymic T cell selection	0.01
	Extrathymic T cell differentiation	0.03

Table 2-1. Specific primer sequence for real-time RT-PCR (Ⅱ).

Gene		Sequence (5′ −>3′)
NOS2	Forward	CAGAGGACCCAGAGACAAGC
	Reverse	TGCTGAAACATTTCCTGTGC
Arginase-1	Forward	GGAATCTGCATGGGCAACCTGTGT
	Reverse	AGGGTCTACGTCTCGCAAGCCA
CD206	Forward	TTCGGTGGACTGTGGACGAGCA
	Reverse	ATAAGCCACCTGCCACTCCGGT
YM-1	Forward	GGGCATACCTTTATCCTGAG
	Reverse	CCACTGAAGTCATCCATGTC
FIZZ1	Forward	TCCCAGTGAATACTGATGAGA
	Reverse	CCACTCTGGATCTCCCAAGA
β -actin	Forward	TTCCTGGGCATGGAGTCCTGTGG
	Reverse	CGCCTAGAAGCATTTGCGGTGG

Table 2-2. The numbers of axillary LN metastasis.

	Control mice (n=7)	BPA mice (n=7)	P-value
Metastatic LN/total LN	3/14	10/14	0.0043

FIGURES

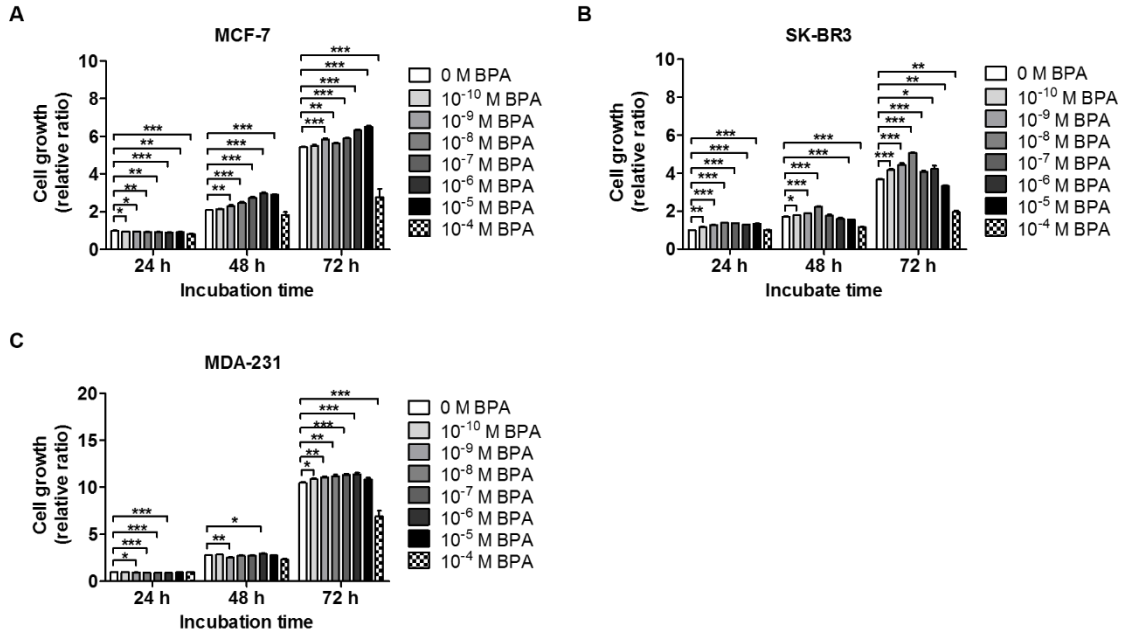

Figure 1-1. Cytotoxic effects of BPA at concentrations ranging from 10^{-10} to 10^{-4} M in MCF-7, SK-BR3 and MDA-MB-231 (MDA-231) cells. A proliferation assay was performed in (A) MCF-7, (B) SK-BR3 and (C) MDA-231 cells treated with different concentrations of BPA ranging from 10^{-10} to 10^{-4} M for 24-72 h using an MTT assay.

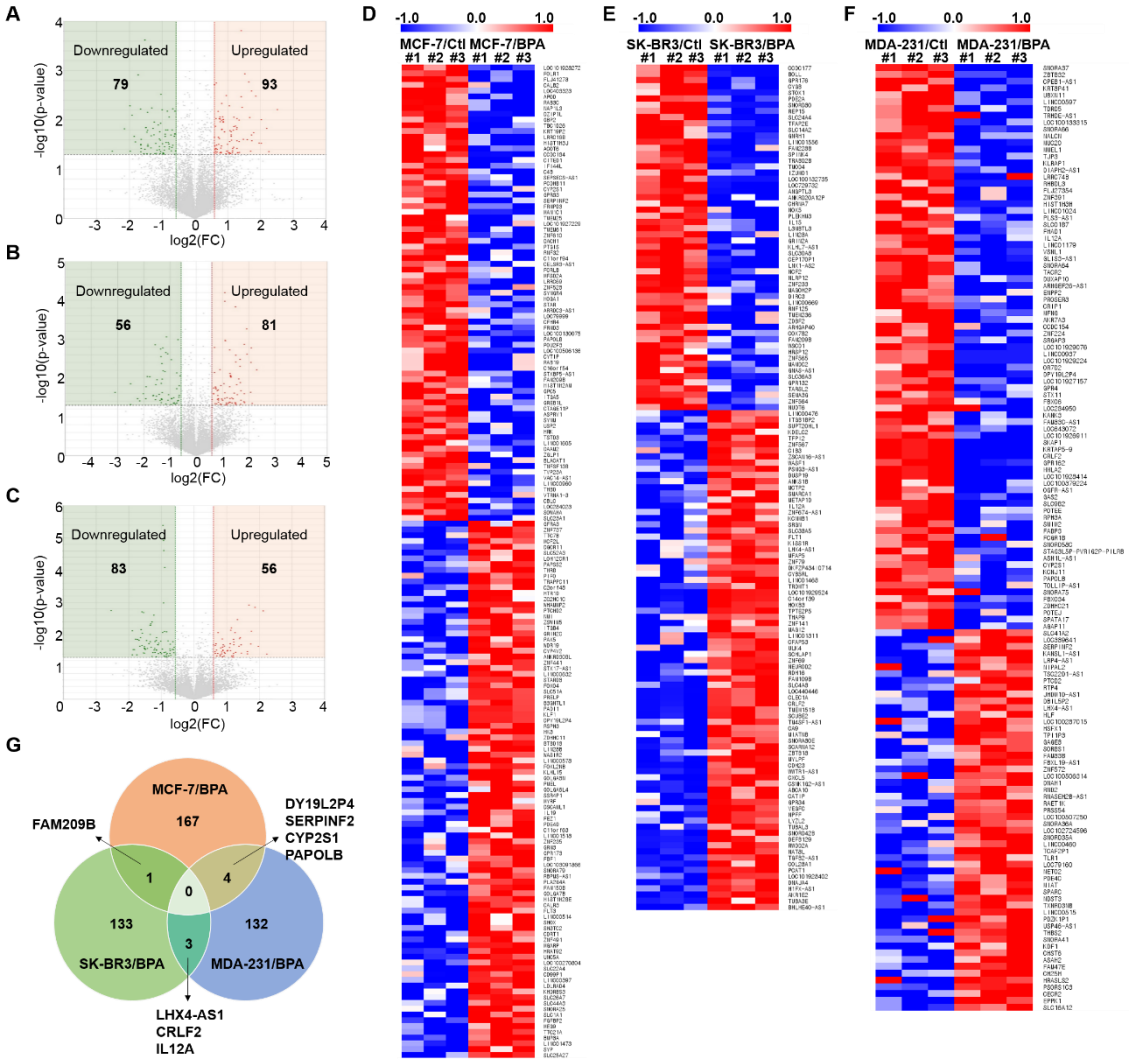

Figure 1-2. Transcriptome profiles of the differentially expressed genes (DEGs) in MCF-7/BPA, SK-BR3/BPA and MDA-MB-231 (MDA-231/BPA) cells relative to the corresponding control samples. (A-C) Volcano plot. The horizontal axis is the log2-fold change (log2FC). The negative log10 of the p-value from the t-test is plotted on the vertical axis. Genes with an absolute fold change of ≥1.5 and a p-value of < 0.05 are indicated by red dots. (D-F) Heat map. The expression patterns of genes with a fold change of ≥1.5 and a p-value of < 0.05 are shown in the heat map generated using TM4-MeV 4.9 software. The heat map indicates upregulation (red) and downregulation (blue). The rows are labeled with individual gene symbols. (G) Venn diagram. The numbers in each circle indicate the number of genes with a fold change of ≥

1.5 and a p−value of < 0.05 in each comparison group, and the number in the overlapping areas is the number of shared genes between two comparison groups. (For interpretation of the references to color in this figure legend, the reader is referred to the web version of this article.)

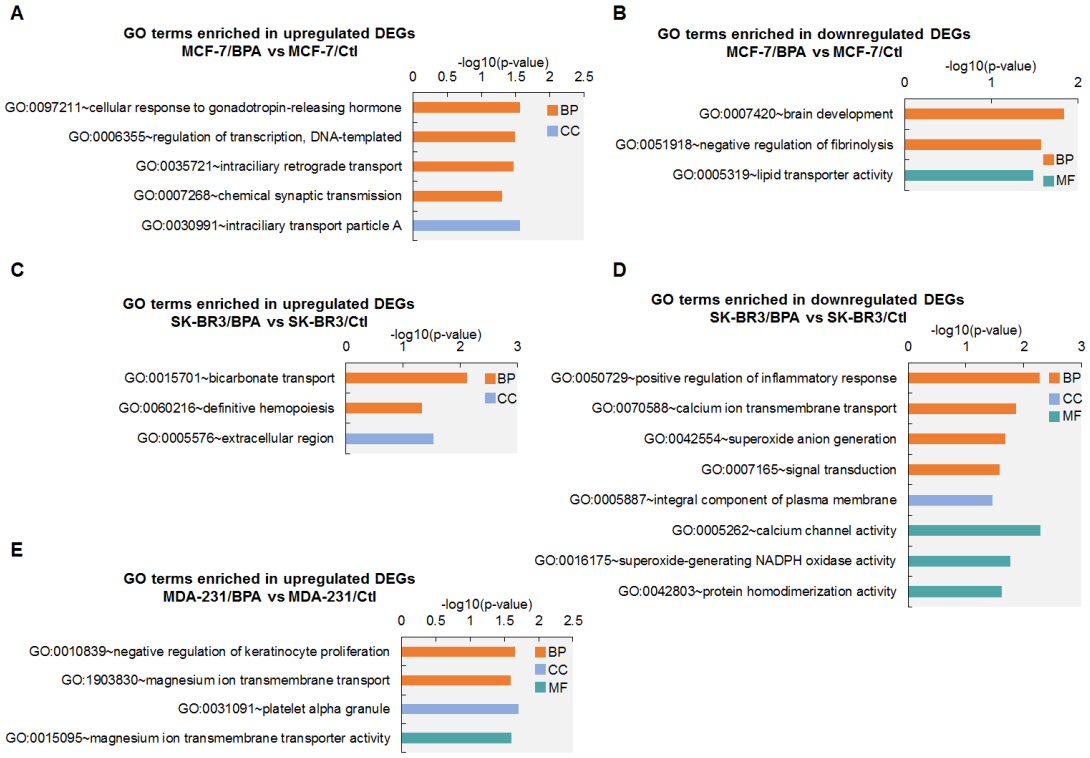

Figure 1−3. Gene Ontology (GO) enrichment analysis. (A−E) The significant GO enrichment of the up− and downregulated genes with an absolute fold change of ≥ 1.5 and a p−value of < 0.05 in biological process (BP), cellular component (CC), and molecular function (MF) terms in MCF−7/BPA, SK−BR3/BPA, and MDA−MB−231 (MDA−231/BPA) cells relative to the corresponding control samples are shown.

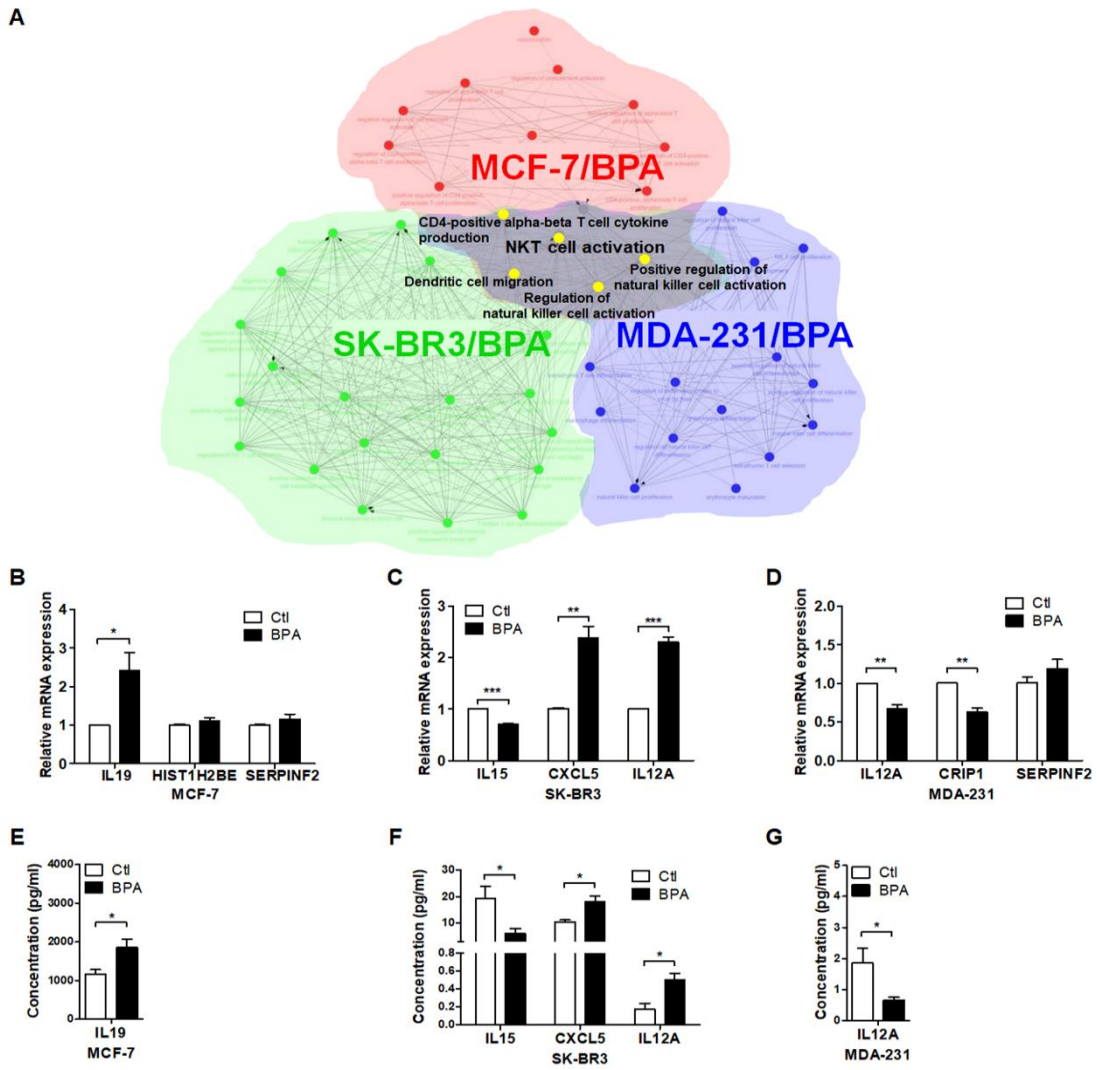

Figure 1−4. Selection of genes annotated within the immune network. (A) A functionally organized Gene Ontology (GO) term network for DEGs belonging to immunityrelated terms across MCF−7/BPA, SK−BR3/BPA and MDA−MB−231/BPA (MDA−231) cells was generated using the Cytoscape tool with the ClueGO plugin. (B−D) qRT−PCR validation of DEGs (HIST1H2BE, IL19, SERPINF2, IL15, CXCL5, IL12A, CRIP1) associated with immunity and inflammation in MCF−7/BPA, SK−BR3/BPA and MDA−231/BPA cells and the corresponding control samples. (E−G) ELISA validation of IL19, IL15, CXCL5, and IL12A protein levels in MCF−7/BPA, SK−BR3/BPA and MDA−231/BPA cells and the corresponding control samples. The data are presented as the means ± standard errors, and experiments were performed in triplicate. *p < .05, **p < .01, ***p < .001.

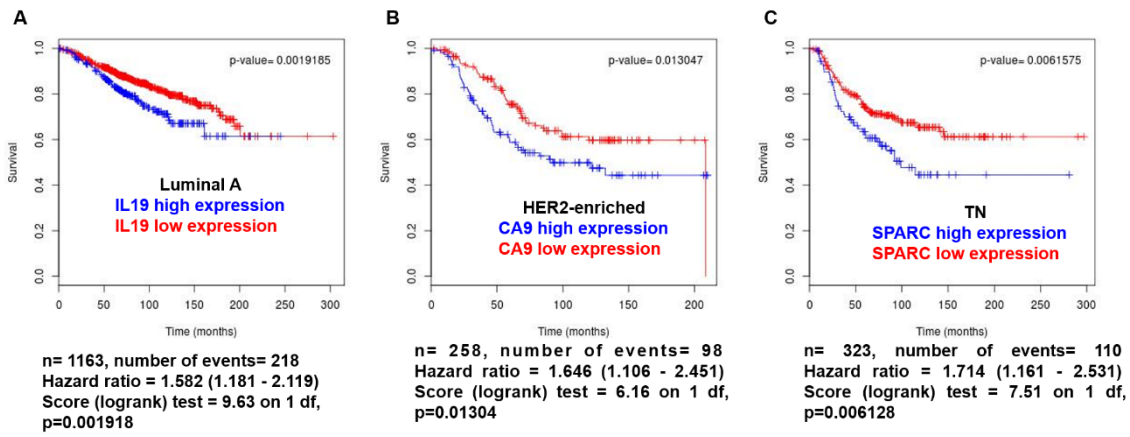

Figure 1-5. Kaplan-Meier plots of overall survival (OS) analysis for breast cancer patients in the BreastMark dataset. (A) The overall survival curve of IL19 in luminal A breast cancer patients. (B) The overall survival curve of CA9 in HER2-enriched breast cancer patients. (C) The overall survival curve of SPARC in TN breast cancer patients.

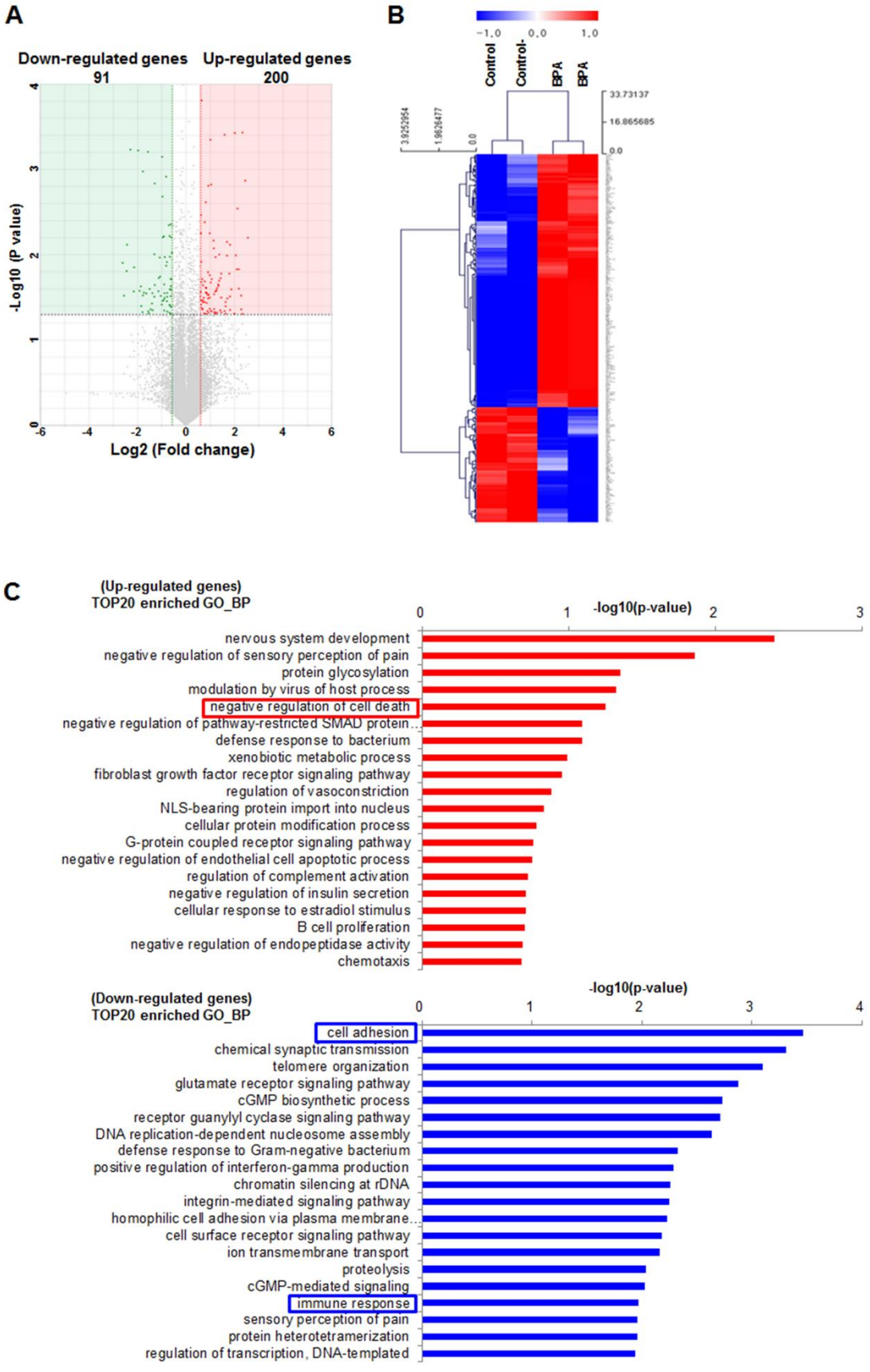

Figure 2-1. Differentially expressed genes (DEGs) clusters and Gene ontology

(GO) categorization between bisphenol A (BPA)−exposed DCIS.com cells and control. (A) Volcano plot of DEGs. Dots on either end of the upper part of the plot indicate genes with statistically significant changes in gene expression. (B) Heatmap reflected expression profiles of DEGs. (C) Top 20 enriched GO terms in downregulated and upregulated genes in BPA−exposed DCIS.com cells. The expression profile of the entire list of the DEGs was used as input data in GO analysis using DAVID database.

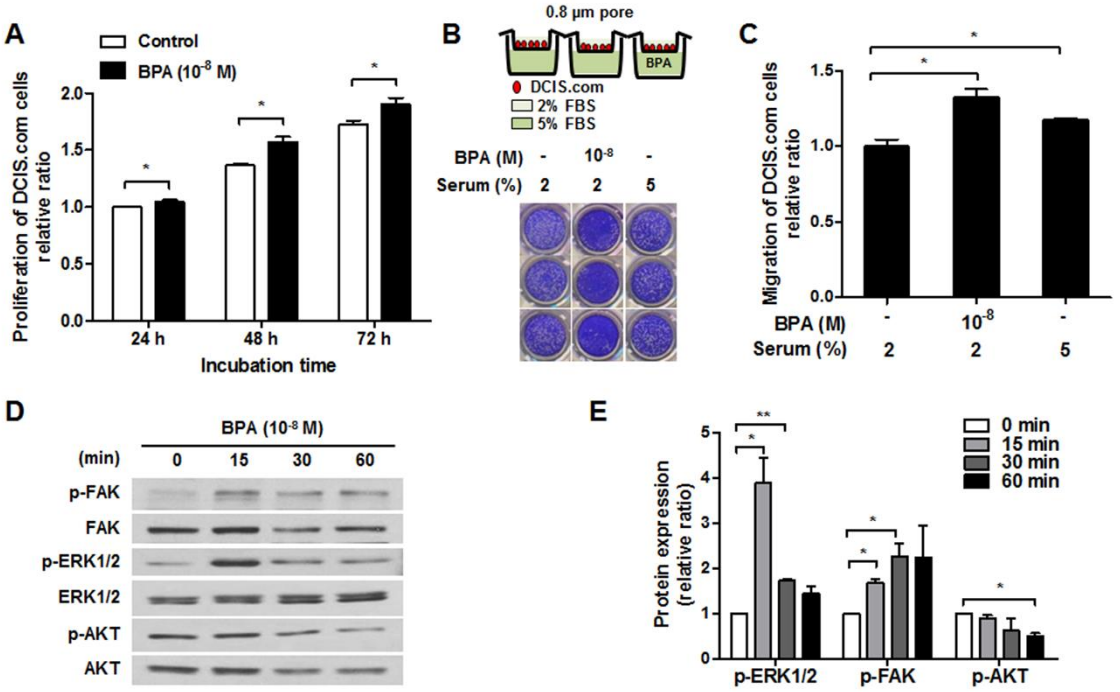

Figure 2-2. Bisphenol A (BPA) promotes the proliferation and migration capacities of DCIS.com cells. (A) Proliferation assay of DCIS.com cells cultured in the presence or absence of 10^{-8} M BPA for 24, 48, and 72 h using 3-(4, 5-dimethylthiazol-2-yl)-2, 5-diphenyl tetrazolium bromide (MTT) assay. (B) Migration assay of DCIS.com cells cultured in the presence or absence of 108 M BPA for 72 h using transwell migration assay. Representative crystal violet staining of migrated DCIS.com cells. (C) Relative quantification of migrated DCIS.com cells using crystal violet assay. (D) Phosphorylation of FAK, AKT, and ERK1/2 in DCIS.com cells treated with 10^{-8} M BPA for 15, 30, and 60min. Representative Western blot phosphorylated or total FAK, AKT, and ERK1/2 of DCIS.com cells. E, Relative quantification of phosphorylated FAK, AKT, and ERK1/2 proteins. All experiments were performed in triplicate for each condition and repeated at least 3 times. Values are reported as the means 6 standard error. *p < .05, **p < .01, ***p<.001

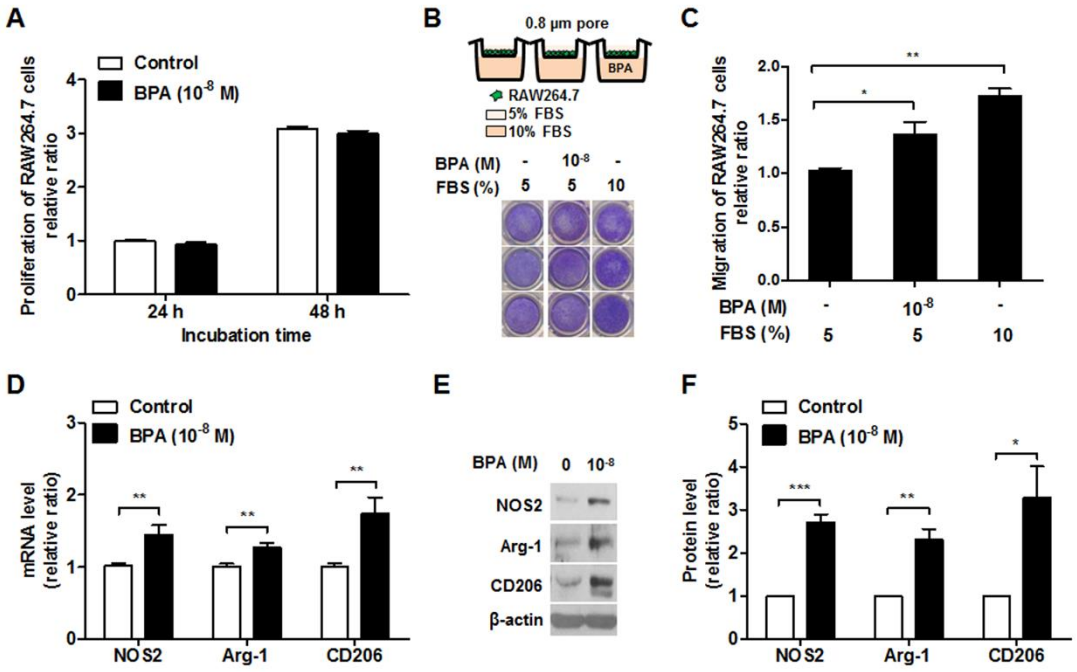

Figure 2-3. Bisphenol A (BPA) promotes the migration ability of RAW264.7 cells and upregulates NOS2, Arg-1, and CD206. (A) Proliferation assay of RAW264.7 cells cultivated in the presence or absence of 10^{-8} M BPA for 24 and 48 h using 3-(4, 5-dimethylthiazol-2-yl)-2, 5-diphenyl tetrazolium bromide (MTT) assay. (B) Migration assay of RAW264.7 cells cultured in the presence or absence of 10^{-8} M BPA for 48 h using transwell migration assay. Representative crystal violet staining of migrated RAW264.7 cells. (C) Relative quantification of migrated RAW264.7 cells using crystal violet assay. (D) The evaluation of M1 and M2 polarization markers, NOS2, Arg-1, and CD206 in RAW264.7 cells treated with 10^{-8} M BPA for 24 h using Real-time RT-PCR. E, Representative Western blot for NOS2 and CD206 in RAW264.7 cells treated with 10^{-8} M BPA for 24 h. F, Relative quantification of NOS2, Arg-1, and CD206 proteins. RAW264.7 cells treated with IFN-γ (20 ng/ml) plus TNF-α (20 ng/ml) for 24 h and IL-4 (50 ng/ml) plus IL-13(20 ng/ml) for 72 h was used as M1 and M2 positive controls. All experiments were performed in triplicate for each condition and repeated at least 3 times. Values are reported as the means 6 standard error. *p < .05, **p < .01, ***p < .001.

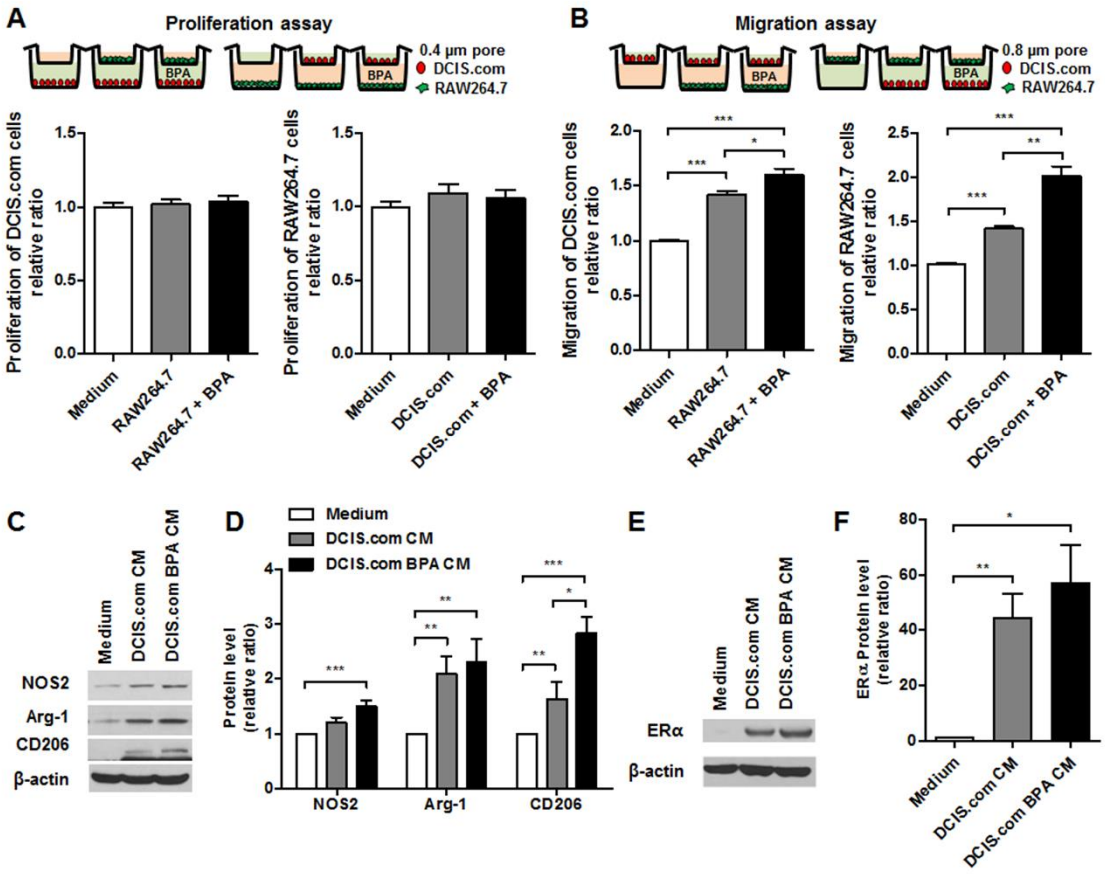

Figure 2-4. Bisphenol A (BPA) augments cell migratory ability and NOS2, Arg-1, and CD206 expression synergistically in coculture system. (A) Proliferation assay of DCIS.com and RAW264.7 cells cultivated in the presence or absence of 10^{-8} M BPA for 72 h in transwell coculture system. (B) Migration assay of DCIS.com and RAW264.7 cells cultivated in presence or absence of 10^{-8} M BPA for 72 h in transwell coculture system. (C) Representative Western blot for NOS2 and CD206 in RAW264.7 cells treated with DCIS.com CM or BPA-exposed DCIS.com CM for 24 h. (D) Relative quantification of NOS2, Arg-1, and CD206 proteins. (E) Representative Western blot for ERα in RAW264.7 cells treated with DCIS.com CM or BPA-exposed DCIS.com CM for 24 h. (F) Relative quantification of ERα proteins. All experiments were performed in triplicate for each condition and repeated at least 3 times. Values are reported as the means 6 standard error. *p < .05, **p < .01, ***p < .001.

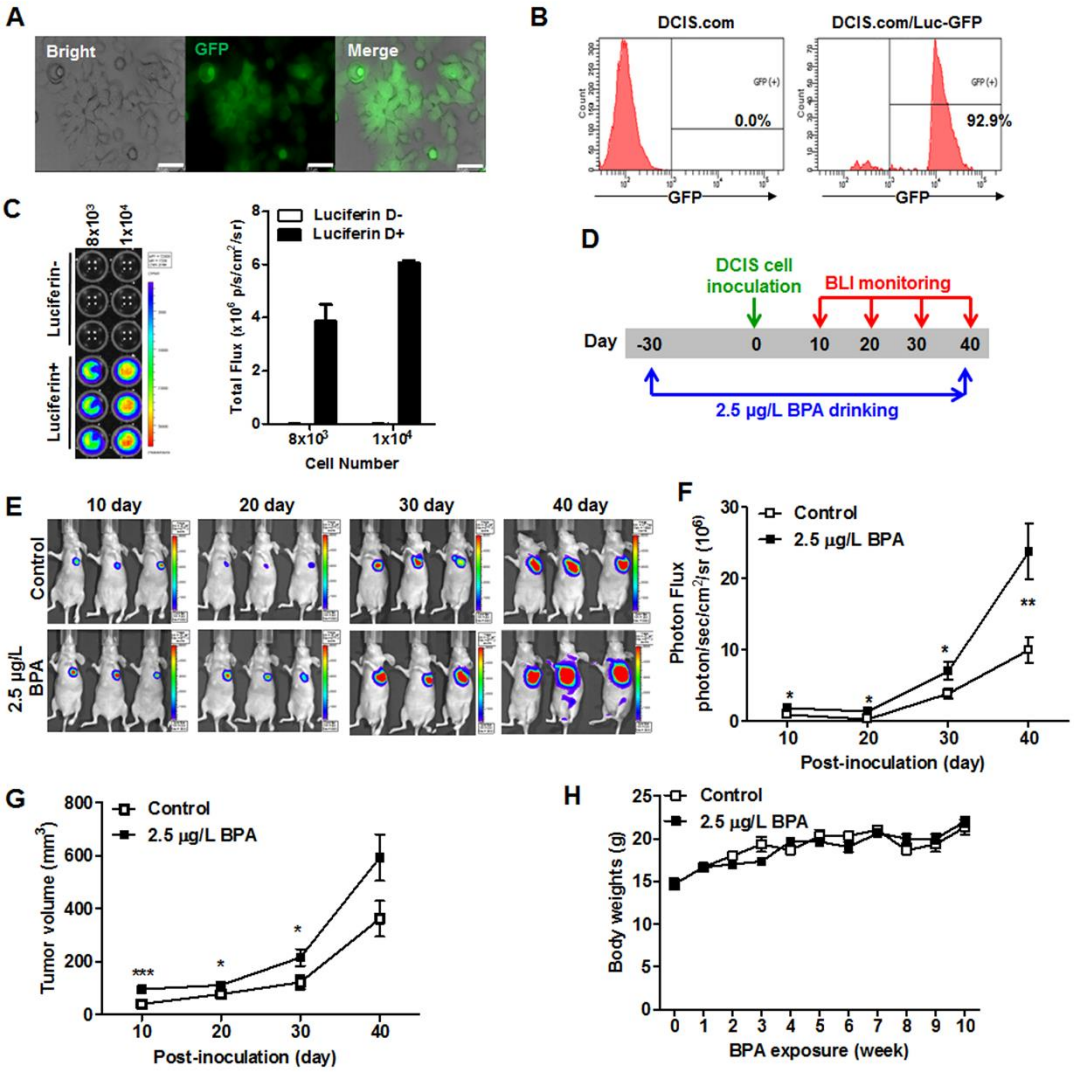

Figure 2-5. Chronic exposure of bisphenol A (BPA) promotes the DCIS tumor growth. (A) Representative fluorescence images of green fluorescence protein (GFP) in DCIS.com/Luc-GFP cells. Scale bar; 50 μm. (B) Histogram analysis of GFP fluorescence in DCIS.com/Luc-GFP cells. (C) Representative in vitro bioluminescence imaging and quantification of bioluminescent signal emitted from 8×10^3 and 1×10^4 of DCIS.com/Luc-GFP cells. (D) Schematic of experimental design for treatments of BPA and assessment of tumor growth in the DCIS xenograft model. (E) Representative bioluminescence imaging of DCIS tumors in 2.5 μg/L BPA-exposed and unexposed control mice at post-inoculation day 10, 20, 30 and 40 days. (F) Quantification of bioluminescent signal emitted from DCIS tumors of 2.5 μg/l BPA-exposed and unexposed

control mice at post-inoculation day 10, 20, 30, and 40 days. (G) Tumor volumes of 2.5 μg/l BPA-exposed and unexposed control mice at post-inoculation day 10, 20, 30, and 40 days. (H) Body weights of experimental mice every week after exposure to 2.5 μg/l BPA. In vivo analysis was performed in 7 mice of each group. Values are reported as the means 6 standard error. *p < .05, **p < .01, ***p < .001.

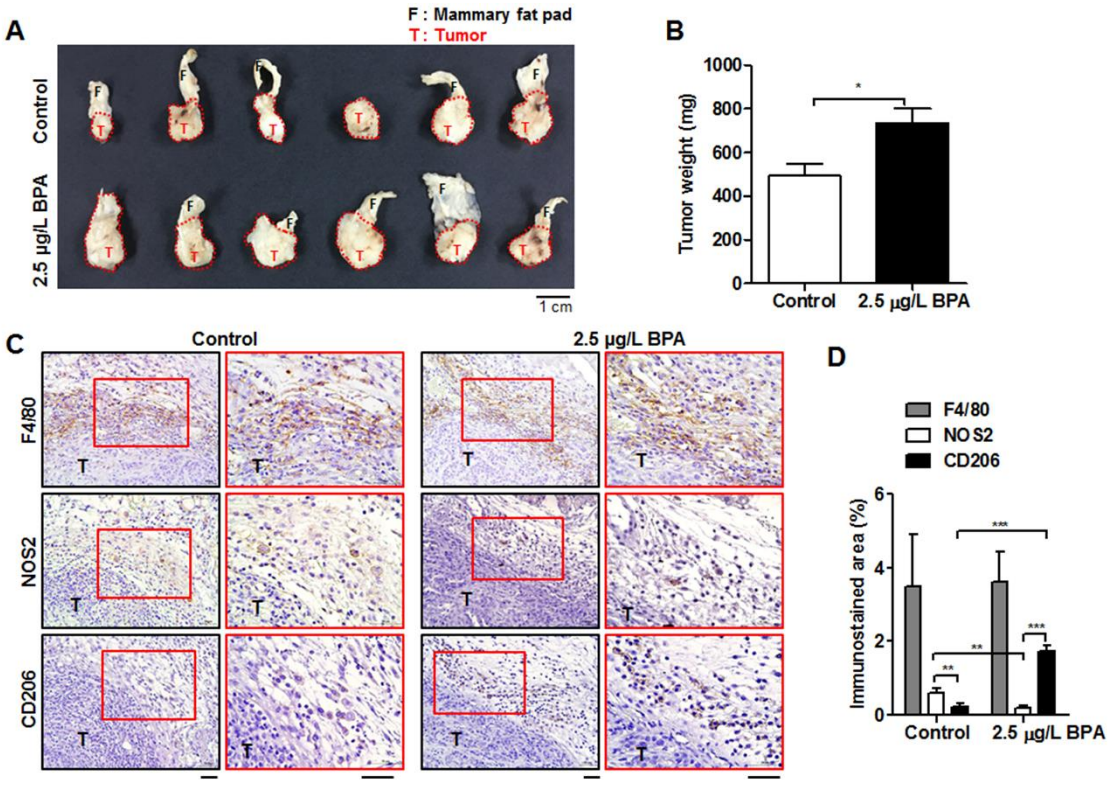

Figure 2-6. Chronic exposure of bisphenol A (BPA) increased CD206+M2 TAM polarization in DCIS tumor microenvironment. (A) Gross images of the tumors removed from mice in 2.5 μg/l BPA-exposed and unexposed control mice at postinoculation day 40. Bar = 1 cm. (B) Average wet weight of tumors removed from 2.5 μg/l BPA-exposed and unexposed control mice at postinoculation day 40. (C) Representative IHC images for F4/80, NOS2, and CD206 on microsections of ductal carcinoma in situ (DCIS) tumors removed from 2.5 μg/l BPA-exposed and unexposed control mice. Scale bar: 50 mm. (D) Quantification of F4/80-, NOS2-, and CD206- immunostained cells as the percentage of brown-stained area in each microphotograph of tumor microsections of 2.5 μg/l BPA-exposed and unexposed control mice. Arrows: NOS2- and CD206-positive cells. All analysis was performed in 7 tumors of each group and the values are reported as the means 6 standard error. *p < .05, **p < .01, ***p < .001.

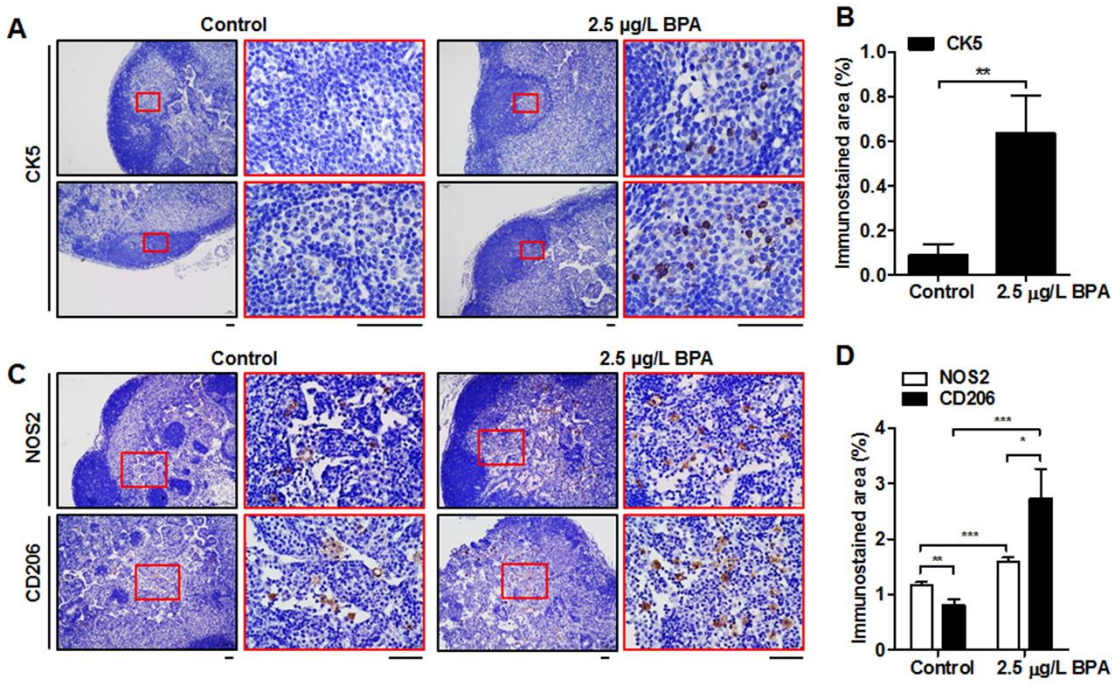

Figure 2-7. Exposure of bisphenol A (BPA) accelerates LN metastasis along with increased CD206+M2 TAM polarization in ductal carcinoma in situ (DCIS) models. (A) Representative IHC images for CK5 on microsections of axillary LN removed from 2.5 μg/l BPA-exposed and unexposed control mice. Scale bar: 50 mm. (B) Quantification of CK5-immunostained cells as the percentage of brown-stained area in each microphotograph of tumor microsections. (C) Representative IHC images for NOS2 and CD206 on microsections of axillary LN removed from 2.5 μg/l BPA-exposed mice and unexposed control mice. Arrows: NOS2- and CD206-positive cells. Scale bar: 50 μm. (D) Quantification of NOS2- and CD206-immunostained cells as the percentage of brown-stained area in each microphotograph of tumor microsections. IHC analysis was performed in 14 axillary LNs of each group and the values are reported as the means 6 standard error. *p < .05, **p < .01, ***p < .001.

REFERENCES

1. Zoeller RT, Brown TR, Doan LL, Gore AC, Skakkebaek NE, Soto AM, et al. Endocrine-disrupting chemicals and public health protection: a statement of principles from The Endocrine Society. Endocrinology 2012;153:4097-110.
2. Rochester JR. Bisphenol A and human health: a review of the literature. Reprod Toxicol 2013;42:132-55.
3. Nagel SC, Bromfield JJ. Bisphenol a: a model endocrine disrupting chemical with a new potential mechanism of action. Endocrinology 2013;154:1962-4.
4. Acconcia F, Pallottini V, Marino M. Molecular Mechanisms of Action of BPA. Dose Response 2015;13:1559325815610582.
5. Rezg R, El-Fazaa S, Gharbi N, Mornagui B. Bisphenol A and human chronic diseases: current evidences, possible mechanisms, and future perspectives. Environ Int 2014;64:83-90.
6. Dairkee SH, Seok J, Champion S, Sayeed A, Mindrinos M, Xiao W, et al. Bisphenol A induces a profile of tumor aggressiveness in high-risk cells from breast cancer patients. Cancer Res 2008;68:2076-80.
7. Yang M, Ryu JH, Jeon R, Kang D, Yoo KY. Effects of bisphenol A on breast cancer and its risk factors. Arch Toxicol 2009;83:281-5.
8. Soto AM, Brisken C, Schaeberle C, Sonnenschein C. Does cancer start in the womb? altered mammary gland development and predisposition to breast cancer due to in utero exposure to endocrine disruptors. J Mammary Gland Biol Neoplasia 2013;18:199-208.
9. Paulose T, Speroni L, Sonnenschein C, Soto AM. Estrogens in the wrong place at the wrong time: Fetal BPA exposure and mammary cancer. Reprod Toxicol 2015;54:58-65.
10. Wang Z, Liu H, Liu S. Low-Dose Bisphenol A Exposure: A Seemingly Instigating Carcinogenic Effect on Breast Cancer. Adv Sci (Weinh) 2017;4:1600248.
11. Vandenberg LN, Maffini MV, Sonnenschein C, Rubin BS, Soto AM. Bisphenol-A and the great divide: a review of controversies in the field of endocrine disruption. Endocr Rev 2009;30:75-95.
12. Jenkins S, Wang J, Eltoum I, Desmond R, Lamartiniere CA. Chronic oral exposure to bisphenol A results in a nonmonotonic dose response in mammary carcinogenesis and metastasis in MMTV-erbB2 mice. Environ Health Perspect 2011;119:1604-9.
13. Lakind JS, Naiman DQ. Bisphenol A (BPA) daily intakes in the United States: estimates from the 2003-2004 NHANES urinary BPA data. J Expo Sci Environ Epidemiol 2008;18:608-15.

14. Seachrist DD, Bonk KW, Ho SM, Prins GS, Soto AM, Keri RA. A review of the carcinogenic potential of bisphenol A. Reprod Toxicol 2016;59:167-82.
15. Kim H, Kim HS, Piao YJ, Moon WK. Bisphenol A promotes the invasive and metastatic potential of ductal carcinoma in situ and pro-tumorigenic polarization of macrophages. Toxicol Sci 2019.
16. Bertucci F, Houlgatte R, Benziane A, Granjeaud S, Adelaide J, Tagett R, et al. Gene expression profiling of primary breast carcinomas using arrays of candidate genes. Hum Mol Genet 2000;9:2981-91.
17. Sauer SJ, Tarpley M, Shah I, Save AV, Lyerly HK, Patierno SR, et al. Bisphenol A activates EGFR and ERK promoting proliferation, tumor spheroid formation and resistance to EGFR pathway inhibition in estrogen receptor-negative inflammatory breast cancer cells. Carcinogenesis 2017;38:252-60.
18. Denkert C. The immunogenicity of breast cancer--molecular subtypes matter. Ann Oncol 2014;25:1453-5.
19. Anders CK, Abramson V, Tan T, Dent R. The Evolution of Triple-Negative Breast Cancer: From Biology to Novel Therapeutics. Am Soc Clin Oncol Educ Book 2016;35:34-42.
20. Mesnage R, Phedonos A, Arno M, Balu S, Corton JC, Antoniou MN. Editor's Highlight: Transcriptome Profiling Reveals Bisphenol A Alternatives Activate Estrogen Receptor Alpha in Human Breast Cancer Cells. Toxicol Sci 2017;158:431-43.
21. Gentleman RC, Carey VJ, Bates DM, Bolstad B, Dettling M, Dudoit S, et al. Bioconductor: open software development for computational biology and bioinformatics. Genome Biol 2004;5:R80.
22. Livak KJ, Schmittgen TD. Analysis of relative gene expression data using real-time quantitative PCR and the 2(-Delta Delta C(T)) Method. Methods 2001;25:402-8.
23. Madden SF, Clarke C, Gaule P, Aherne ST, O'Donovan N, Clynes M, et al. BreastMark: an integrated approach to mining publicly available transcriptomic datasets relating to breast cancer outcome. Breast Cancer Res 2013;15:R52.
24. Vandenberg LN. Non-monotonic dose responses in studies of endocrine disrupting chemicals: bisphenol a as a case study. Dose Response 2014;12:259-76.
25. Yin R, Gu L, Li M, Jiang C, Cao T, Zhang X. Gene expression profiling analysis of bisphenol A-induced perturbation in biological processes in ER-negative HEK293 cells. PLoS One 2014;9:e98635.
26. Gao H, Yang BJ, Li N, Feng LM, Shi XY, Zhao WH, et al. Bisphenol A and hormone-associated cancers: current progress and perspectives. Medicine (Baltimore) 2015;94:e211.

27. Murata M, Kang JH. Bisphenol A (BPA) and cell signaling pathways. Biotechnol Adv 2018;36:311-27.
28. Dong S, Terasaka S, Kiyama R. Bisphenol A induces a rapid activation of Erk1/2 through GPR30 in human breast cancer cells. Environ Pollut 2011;159:212-8.
29. Castillo Sanchez R, Gomez R, Perez Salazar E. Bisphenol A Induces Migration through a GPER-, FAK-, Src-, and ERK2-Dependent Pathway in MDA-MB-231 Breast Cancer Cells. Chem Res Toxicol 2016;29:285-95.
30. Caceres M, Guerrero J, Martinez J. Overexpression of RhoA-GTP induces activation of the Epidermal Growth Factor Receptor, dephosphorylation of focal adhesion kinase and increased motility in breast cancer cells. Exp Cell Res 2005;309:229-38.
31. Li H, Ung CY, Ma XH, Li BW, Low BC, Cao ZW, et al. Simulation of crosstalk between small GTPase RhoA and EGFR-ERK signaling pathway via MEKK1. Bioinformatics 2009;25:358-64.
32. Xu F, Wang X, Wu N, He S, Yi W, Xiang S, et al. Bisphenol A induces proliferative effects on both breast cancer cells and vascular endothelial cells through a shared GPER-dependent pathway in hypoxia. Environ Pollut 2017;231:1609-20.
33. von Alten J, Fister S, Schulz H, Viereck V, Frosch KH, Emons G, et al. GnRH analogs reduce invasiveness of human breast cancer cells. Breast Cancer Res Treat 2006;100:13-21.
34. Aguilar-Rojas A, Huerta-Reyes M, Maya-Nunez G, Arechavaleta-Velasco F, Conn PM, Ulloa-Aguirre A, et al. Gonadotropin-releasing hormone receptor activates GTPase RhoA and inhibits cell invasion in the breast cancer cell line MDA-MB-231. BMC Cancer 2012;12:550.
35. Robertson JF, Blamey RW. The use of gonadotrophin-releasing hormone (GnRH) agonists in early and advanced breast cancer in pre- and perimenopausal women. Eur J Cancer 2003;39:861-9.
36. Zorio E, Gilabert-Estelles J, Espana F, Ramon LA, Cosin R, Estelles A. Fibrinolysis: the key to new pathogenetic mechanisms. Curr Med Chem 2008;15:923-9.
37. Dowling P, Palmerini V, Henry M, Meleady P, Lynch V, Ballot J, et al. Transferrin-bound proteins as potential biomarkers for advanced breast cancer patients. BBA Clin 2014;2:24-30.
38. Paquet-Fifield S, Roufail S, Zhang YF, Sofian T, Byrne DJ, Coughlin PB, et al. The fibrinolysis inhibitor alpha2-antiplasmin restricts lymphatic remodelling and metastasis in a mouse model of cancer. Growth Factors 2017;35:61-75.
39. Bazzi ZA, Lanoue D, El-Youssef M, Romagnuolo R, Tubman J, Cavallo-Medved D, et al. Activated thrombin-activatable fibrinolysis inhibitor (TAFIa) attenuates breast cancer cell metastatic behaviors through inhibition of plasminogen activation and extracellular proteolysis. BMC Cancer 2016;16:328.

40. Gorbatenko A, Olesen CW, Morup N, Thiel G, Kallunki T, Valen E, et al. ErbB2 upregulates the Na+,HCO3(-)-cotransporter NBCn1/SLC4A7 in human breast cancer cells via Akt, ERK, Src, and Kruppel-like factor 4. FASEB J 2014;28:350-63.
41. Hanahan D, Weinberg RA. Hallmarks of cancer: the next generation. Cell 2011;144:646-74.
42. Maurice DH, Ke H, Ahmad F, Wang Y, Chung J, Manganiello VC. Advances in targeting cyclic nucleotide phosphodiesterases. Nat Rev Drug Discov 2014;13:290-314.
43. Trabanco AA, Buijnsters P, Rombouts FJ. Towards selective phosphodiesterase 2A (PDE2A) inhibitors: a patent review (2010 - present). Expert Opin Ther Pat 2016;26:933-46.
44. Steel JC, Waldmann TA, Morris JC. Interleukin-15 biology and its therapeutic implications in cancer. Trends Pharmacol Sci 2012;33:35-41.
45. Ellis J, Anlauf H, Kurten S, Lozano-Cortes D, Alsaffar Z, Curdia J, et al. Cross shelf benthic biodiversity patterns in the Southern Red Sea. Sci Rep 2017;7:437.
46. Lee S, Kong Y, Weatherbee SD. Forward genetics identifies Kdf1/1810019J16Rik as an essential regulator of the proliferation-differentiation decision in epidermal progenitor cells. Dev Biol 2013;383:201-13.
47. Yoshida T, Shiraki N, Baba H, Goto M, Fujiwara S, Kume K, et al. Expression patterns of epiplakin1 in pancreas, pancreatic cancer and regenerating pancreas. Genes Cells 2008;13:667-78.
48. Uddin MB, Balaravi Pillai B, Tha KK, Ashaie M, Karim ME, Chowdhury EH. Carbonate Apatite Nanoparticles-Facilitated Intracellular Delivery of siRNA(s) Targeting Calcium Ion Channels Efficiently Kills Breast Cancer Cells. Toxics 2018;6.
49. Sasahira T, Nishiguchi Y, Kurihara-Shimomura M, Nakashima C, Kuniyasu H, Kirita T. NIPA-like domain containing 1 is a novel tumor-promoting factor in oral squamous cell carcinoma. J Cancer Res Clin Oncol 2018;144:875-82.
50. Glunde K, Bhujwalla ZM, Ronen SM. Choline metabolism in malignant transformation. Nat Rev Cancer 2011;11:835-48.
51. Chen M, Zhou K, Chen X, Qiao S, Hu Y, Xu B, et al. Metabolomic analysis reveals metabolic changes caused by bisphenol A in rats. Toxicol Sci 2014;138:256-67.
52. Prickett TD, Samuels Y. Molecular pathways: dysregulated glutamatergic signaling pathways in cancer. Clin Cancer Res 2012;18:4240-6.
53. Fazzari J, Lin H, Murphy C, Ungard R, Singh G. Inhibitors of glutamate release from breast cancer cells; new targets for cancer-induced bone-pain. Sci Rep 2015;5:8380.

54. Mandoj C, Pizzuti L, Sergi D, Sperduti I, Mazzotta M, Di Lauro L, et al. Observational study of coagulation activation in early breast cancer: development of a prognostic model based on data from the real world setting. J Transl Med 2018;16:129.
55. Blancher C, Moore JW, Talks KL, Houlbrook S, Harris AL. Relationship of hypoxia-inducible factor (HIF)-1alpha and HIF-2alpha expression to vascular endothelial growth factor induction and hypoxia survival in human breast cancer cell lines. Cancer Res 2000;60:7106-13.
56. Ye IC, Fertig EJ, DiGiacomo JW, Considine M, Godet I, Gilkes DM. Molecular Portrait of Hypoxia in Breast Cancer: A Prognostic Signature and Novel HIF-Regulated Genes. Mol Cancer Res 2018;16:1889-901.
57. Cai FF, Xu C, Pan X, Cai L, Lin XY, Chen S, et al. Prognostic value of plasma levels of HIF-1a and PGC-1a in breast cancer. Oncotarget 2016;7:77793-806.
58. Jarman EJ, Ward C, Turnbull AK, Martinez-Perez C, Meehan J, Xintaropoulou C, et al. HER2 regulates HIF-2alpha and drives an increased hypoxic response in breast cancer. Breast Cancer Res 2019;21:10.
59. Shalapour S, Karin M. Immunity, inflammation, and cancer: an eternal fight between good and evil. J Clin Invest 2015;125:3347-55.
60. Xu J, Huang G, Guo TL. Developmental Bisphenol A Exposure Modulates Immune-Related Diseases. Toxics 2016;4.
61. Dias S, Boyd R, Balkwill F. IL-12 regulates VEGF and MMPs in a murine breast cancer model. Int J Cancer 1998;78:361-5.
62. Colombo MP, Trinchieri G. Interleukin-12 in anti-tumor immunity and immunotherapy. Cytokine Growth Factor Rev 2002;13:155-68.
63. Roszak A, Mostowska A, Sowinska A, Lianeri M, Jagodzinski PP. Contribution of IL12A and IL12B polymorphisms to the risk of cervical cancer. Pathol Oncol Res 2012;18:997-1002.
64. Begley LA, Kasina S, Mehra R, Adsule S, Admon AJ, Lonigro RJ, et al. CXCL5 promotes prostate cancer progression. Neoplasia 2008;10:244-54.
65. Hsing CH, Cheng HC, Hsu YH, Chan CH, Yeh CH, Li CF, et al. Upregulated IL-19 in breast cancer promotes tumor progression and affects clinical outcome. Clin Cancer Res 2012;18:713-25.
66. Ludyga N, Englert S, Pflieger K, Rauser S, Braselmann H, Walch A, et al. The impact of cysteine-rich intestinal protein 1 (CRIP1) in human breast cancer. Mol Cancer 2013;12:28.
67. Span PN, Bussink J, Manders P, Beex LV, Sweep CG. Carbonic anhydrase-9 expression levels and prognosis in human breast cancer: association with treatment outcome. Br J Cancer 2003;89:271-6.

68. Rosset EM, Bradshaw AD. SPARC/osteonectin in mineralized tissue. Matrix Biol 2016;52-54:78-87.
69. Watkins G, Douglas-Jones A, Bryce R, Mansel RE, Jiang WG. Increased levels of SPARC (osteonectin) in human breast cancer tissues and its association with clinical outcomes. Prostaglandins Leukot Essent Fatty Acids 2005;72:267-72.
70. Burstein HJ, Polyak K, Wong JS, Lester SC, Kaelin CM. Ductal carcinoma in situ of the breast. N Engl J Med 2004;350:1430-41.
71. Kerlikowske K, Molinaro A, Cha I, Ljung BM, Ernster VL, Stewart K, et al. Characteristics associated with recurrence among women with ductal carcinoma in situ treated by lumpectomy. J Natl Cancer Inst 2003;95:1692-702.
72. Carron EC, Homra S, Rosenberg J, Coffelt SB, Kittrell F, Zhang Y, et al. Macrophages promote the progression of premalignant mammary lesions to invasive cancer. Oncotarget 2017;8:50731-46.
73. Pollard JW. Macrophages define the invasive microenvironment in breast cancer. J Leukoc Biol 2008;84:623-30.
74. Reeves GK, Pirie K, Green J, Bull D, Beral V, Million Women Study C. Comparison of the effects of genetic and environmental risk factors on in situ and invasive ductal breast cancer. Int J Cancer 2012;131:930-7.
75. Calafat AM, Ye X, Wong LY, Reidy JA, Needham LL. Exposure of the U.S. population to bisphenol A and 4-tertiary-octylphenol: 2003-2004. Environ Health Perspect 2008;116:39-44.
76. Campbell L, Emmerson E, Williams H, Saville CR, Krust A, Chambon P, et al. Estrogen receptor-alpha promotes alternative macrophage activation during cutaneous repair. J Invest Dermatol 2014;134:2447-57.
77. Diamanti-Kandarakis E, Bourguignon JP, Giudice LC, Hauser R, Prins GS, Soto AM, et al. Endocrine-disrupting chemicals: an Endocrine Society scientific statement. Endocr Rev 2009;30:293-342.
78. Munoz-de-Toro M, Markey CM, Wadia PR, Luque EH, Rubin BS, Sonnenschein C, et al. Perinatal exposure to bisphenol-A alters peripubertal mammary gland development in mice. Endocrinology 2005;146:4138-47.
79. Murray TJ, Maffini MV, Ucci AA, Sonnenschein C, Soto AM. Induction of mammary gland ductal hyperplasias and carcinoma in situ following fetal bisphenol A exposure. Reprod Toxicol 2007;23:383-90.
80. Vandenberg LN, Maffini MV, Schaeberle CM, Ucci AA, Sonnenschein C, Rubin BS, et al. Perinatal exposure to the xenoestrogen bisphenol-A induces mammary intraductal hyperplasias in adult CD-1 mice. Reprod Toxicol 2008;26:210-9.

81. Acevedo N, Davis B, Schaeberle CM, Sonnenschein C, Soto AM. Perinatally administered bisphenol a as a potential mammary gland carcinogen in rats. Environ Health Perspect 2013;121:1040-6.
82. Schug TT, Janesick A, Blumberg B, Heindel JJ. Endocrine disrupting chemicals and disease susceptibility. J Steroid Biochem Mol Biol 2011;127:204-15.
83. Liu Y, Mei C, Liu H, Wang H, Zeng G, Lin J, et al. Modulation of cytokine expression in human macrophages by endocrine-disrupting chemical Bisphenol-A. Biochem Biophys Res Commun 2014;451:592-8.
84. Malaise Y, Menard S, Cartier C, Lencina C, Sommer C, Gaultier E, et al. Consequences of bisphenol a perinatal exposure on immune responses and gut barrier function in mice. Arch Toxicol 2018;92:347-58.
85. Pisapia L, Del Pozzo G, Barba P, Caputo L, Mita L, Viggiano E, et al. Effects of some endocrine disruptors on cell cycle progression and murine dendritic cell differentiation. Gen Comp Endocrinol 2012;178:54-63.
86. Yoshino S, Yamaki K, Li X, Sai T, Yanagisawa R, Takano H, et al. Prenatal exposure to bisphenol A up-regulates immune responses, including T helper 1 and T helper 2 responses, in mice. Immunology 2004;112:489-95.
87. Youn JY, Park HY, Lee JW, Jung IO, Choi KH, Kim K, et al. Evaluation of the immune response following exposure of mice to bisphenol A: induction of Th1 cytokine and prolactin by BPA exposure in the mouse spleen cells. Arch Pharm Res 2002;25:946-53.
88. Foxcroft LM, Evans EB, Porter AJ. Difficulties in the pre-operative diagnosis of phyllodes tumours of the breast: a study of 84 cases. Breast 2007;16:27-37.
89. O'Sullivan C, Lewis CE. Tumour-associated leucocytes: friends or foes in breast carcinoma. J Pathol 1994;172:229-35.
90. Georgoudaki AM, Prokopec KE, Boura VF, Hellqvist E, Sohn S, Ostling J, et al. Reprogramming Tumor-Associated Macrophages by Antibody Targeting Inhibits Cancer Progression and Metastasis. Cell Rep 2016;15:2000-11.
91. Sousa S, Brion R, Lintunen M, Kronqvist P, Sandholm J, Monkkonen J, et al. Human breast cancer cells educate macrophages toward the M2 activation status. Breast Cancer Res 2015;17:101.
92. Williams CB, Yeh ES, Soloff AC. Tumor-associated macrophages: unwitting accomplices in breast cancer malignancy. NPJ Breast Cancer 2016;2.
93. Linde N, Casanova-Acebes M, Sosa MS, Mortha A, Rahman A, Farias E, et al. Macrophages orchestrate breast cancer early dissemination and metastasis. Nat Commun 2018;9:21.

94. Piao YJ, Kim HS, Hwang EH, Woo J, Zhang M, Moon WK. Breast cancer cell-derived exosomes and macrophage polarization are associated with lymph node metastasis. Oncotarget 2018;9:7398-410.
95. Aboul Ezz HS, Khadrawy YA, Mourad IM. The effect of bisphenol A on some oxidative stress parameters and acetylcholinesterase activity in the heart of male albino rats. Cytotechnology 2015;67:145-55.
96. Byun JA, Heo Y, Kim YO, Pyo MY. Bisphenol A-induced downregulation of murine macrophage activities in vitro and ex vivo. Environ Toxicol Pharmacol 2005;19:19-24.
97. Gao X, Wang HS. Impact of bisphenol a on the cardiovascular system - epidemiological and experimental evidence and molecular mechanisms. Int J Environ Res Public Health 2014;11:8399-413.
98. Palacios-Arreola MI, Nava-Castro KE, Rio-Araiza VHD, Perez-Sanchez NY, Morales-Montor J. A single neonatal administration of Bisphenol A induces higher tumour weight associated to changes in tumour microenvironment in the adulthood. Sci Rep 2017;7:10573.
99. Quinlan AR, Hall IM. BEDTools: a flexible suite of utilities for comparing genomic features. Bioinformatics 2010;26:841-2.
100. Huang da W, Sherman BT, Lempicki RA. Systematic and integrative analysis of large gene lists using DAVID bioinformatics resources. Nat Protoc 2009;4:44-57.
101. Huang da W, Sherman BT, Lempicki RA. Bioinformatics enrichment tools: paths toward the comprehensive functional analysis of large gene lists. Nucleic Acids Res 2009;37:1-13.
102. Bunda S, Heir P, Metcalf J, Li ASC, Agnihotri S, Pusch S, et al. CIC protein instability contributes to tumorigenesis in glioblastoma. Nat Commun 2019;10:661.
103. Gomez AL, Delconte MB, Altamirano GA, Vigezzi L, Bosquiazzo VL, Barbisan LF, et al. Perinatal Exposure to Bisphenol A or Diethylstilbestrol Increases the Susceptibility to Develop Mammary Gland Lesions After Estrogen Replacement Therapy in Middle-Aged Rats. Horm Cancer 2017;8:78-89.
104. Li Q, Lawrence CR, Nowak RA, Flaws JA, Bagchi MK, Bagchi IC. Bisphenol A and Phthalates Modulate Peritoneal Macrophage Function in Female Mice Involving SYMD2-H3K36 Dimethylation. Endocrinology 2018;159:2216-28.
105. Aris A. Estimation of bisphenol A (BPA) concentrations in pregnant women, fetuses and nonpregnant women in Eastern Townships of Canada. Reprod Toxicol 2014;45:8-13.
106. Olsen L, Lind L, Lind PM. Associations between circulating levels of bisphenol A and phthalate metabolites and coronary risk in the elderly. Ecotoxicol Environ Saf 2012;80:179-83.
107. vom Saal FS, Welshons WV. Evidence that bisphenol A (BPA) can be accurately measured without contamination in human serum and urine,

and that BPA causes numerous hazards from multiple routes of exposure. Mol Cell Endocrinol 2014;398:101-13.
108. Ribeiro E, Ladeira C, Viegas S. Occupational Exposure to Bisphenol A (BPA): A Reality That Still Needs to Be Unveiled. Toxics 2017;5.
109. Chapin RE, Adams J, Boekelheide K, Gray LE, Jr., Hayward SW, Lees PS, et al. NTP-CERHR expert panel report on the reproductive and developmental toxicity of bisphenol A. Birth Defects Res B Dev Reprod Toxicol 2008;83:157-395.
110. Thomas P, Dong J. Binding and activation of the seven-transmembrane estrogen receptor GPR30 by environmental estrogens: a potential novel mechanism of endocrine disruption. J Steroid Biochem Mol Biol 2006;102:175-9.
111. Zhang XL, Liu N, Weng SF, Wang HS. Bisphenol A Increases the Migration and Invasion of Triple-Negative Breast Cancer Cells via Oestrogen-related Receptor Gamma. Basic Clin Pharmacol Toxicol 2016;119:389-95.
112. Behbod F, Kittrell FS, LaMarca H, Edwards D, Kerbawy S, Heestand JC, et al. An intraductal human-in-mouse transplantation model mimics the subtypes of ductal carcinoma in situ. Breast Cancer Res 2009;11:R66.
113. Durando M, Kass L, Piva J, Sonnenschein C, Soto AM, Luque EH, et al. Prenatal bisphenol A exposure induces preneoplastic lesions in the mammary gland in Wistar rats. Environ Health Perspect 2007;115:80-6.
114. Harney AS, Arwert EN, Entenberg D, Wang Y, Guo P, Qian BZ, et al. Real-Time Imaging Reveals Local, Transient Vascular Permeability, and Tumor Cell Intravasation Stimulated by TIE2hi Macrophage-Derived VEGFA. Cancer Discov 2015;5:932-43.
115. Kitamura T, Qian BZ, Soong D, Cassetta L, Noy R, Sugano G, et al. CCL2-induced chemokine cascade promotes breast cancer metastasis by enhancing retention of metastasis-associated macrophages. J Exp Med 2015;212:1043-59.
116. Kasneci A, Lee JS, Yun TJ, Shang J, Lampen S, Gomolin T, et al. From the Cover: Lifelong Exposure of C57bl/6n Male Mice to Bisphenol A or Bisphenol S Reduces Recovery From a Myocardial Infarction. Toxicol Sci 2017;159:189-202.
117. Kou XX, Li CS, He DQ, Wang XD, Hao T, Meng Z, et al. Estradiol promotes M1-like macrophage activation through cadherin-11 to aggravate temporomandibular joint inflammation in rats. J Immunol 2015;194:2810-8.
118. Pyo MY, Kim HJ, Back SK, Yang M. Downregulation of peritoneal macrophage activity in mice exposed to bisphenol A during pregnancy and lactation. Arch Pharm Res 2007;30:1476-81.

119. Segura JJ, Jimenez-Rubio A, Pulgar R, Olea N, Guerrero JM, Calvo JR. In vitro effect of the resin component bisphenol A on substrate adherence capacity of macrophages. J Endod 1999;25:341-4.
120. Toniolo A, Fadini GP, Tedesco S, Cappellari R, Vegeto E, Maggi A, et al. Alternative activation of human macrophages is rescued by estrogen treatment in vitro and impaired by menopausal status. J Clin Endocrinol Metab 2015;100:E50-8.
121. Campbell MJ, Baehner F, O'Meara T, Ojukwu E, Han B, Mukhtar R, et al. Characterizing the immune microenvironment in high-risk ductal carcinoma in situ of the breast. Breast Cancer Res Treat 2017;161:17-28.
122. Esserman LJ, Kumar AS, Herrera AF, Leung J, Au A, Chen YY, et al. Magnetic resonance imaging captures the biology of ductal carcinoma in situ. J Clin Oncol 2006;24:4603-10.
123. Sharma M, Beck AH, Webster JA, Espinosa I, Montgomery K, Varma S, et al. Analysis of stromal signatures in the tumor microenvironment of ductal carcinoma in situ. Breast Cancer Res Treat 2010;123:397-404.
124. Pupo M, Pisano A, Lappano R, Santolla MF, De Francesco EM, Abonante S, et al. Bisphenol A induces gene expression changes and proliferative effects through GPER in breast cancer cells and cancer-associated fibroblasts. Environ Health Perspect 2012;120:1177-82.
125. Chen Y, Xu HS, Guo TL. Modulation of cytokine/chemokine production in human macrophages by bisphenol A: A comparison to analogues and interactions with genistein. J Immunotoxicol 2018;15:96-103.
126. Ricupito A, Del Pozzo G, Diano N, Grano V, Portaccio M, Marino M, et al. Effect of bisphenol A with or without enzyme treatment on the proliferation and viability of MCF-7 cells. Environ Int 2009;35:21-6.

국문초록

서론: 비스페놀A는 폴리카보네이트 플라스틱과 에폭시레진의 기본 원료로 사용되며 일부 감열지 현상제, 플라스틱, 치아밀봉재 등에도 사용되는 유기화합물이다. 구조적으로 여성호르몬인 에스트로겐과 유사하게 작용하여 유방암 발생률을 증가시키는 요인으로 제기되어 왔으나 비스페놀A 노출의 유방암 세포내 전사체 발현에 미치는 영향과 유방암 진행과의 상관관계에 대한 연구는 부족하다. 본 연구의 목적은 다양한 유방암 세포주와 동물모델에서 저용량 비스페놀A의 장기간 노출이 유방암 전사체 발현 변화와 유방암 악성도 촉발에 미치는 영향을 평가하는 것이다.

실험방법: 본 연구는 2개의 독립적인 실험 내용으로 구성되어 있다.

1. 유방암 세포주는 호르몬 수용체 유무에 따라 ER양성 유형인 MCF-7, HER2 과발현 유형인 SK-BR3, 삼중음성 유형인 MDA-MB-231을 사용하였다. 저용량의 장기간 비스페놀A 노출에 관한 전사체 분석은 30일간 10^{-8} M에 노출시킨 각 유방암 세포주들의 RNA를 분리한 후 RNA 염기서열분석을 진행하였고, QuantSeq 3' mRNA-Seq Library Prep Kit를 이용하여 염기서열 라이브러리를 만들었다. 이 라이브러리에서 Bowtie2 소프트웨어를 이용하여 매핑한 후 Bedtool프로그램을 통해 상이 발현 유전자들을 구분하였고 온라인 공개 데이터베이스인 DAVID와 KEGG, PANTHER 등을 통해 기능적 분석을 진행하였다. 또한 세포주들의 상이 발현 유전자 세트간 상호작용에 대한 매핑은 Cytoscape software을 이용하여 분석하였고, 공개 데이터베이스인 BreastMark를 통해 얻은 각 아형별 유방암 환자의 생존율 정보를 활용하여 비스페놀A에 의한 상이 발현 유전자와의 상관관계를 분석하였다.

2. 비스페놀A 노출이 유방암의 진행에 미치는 영향을 확인하기 위해 세포실험에서 유방암 초기단계의 특성을 가지는 관상피내암세포인 MCF10DCIS.com과 종양면역

환경에서 높은 분포도를 보이며 다양한 역할을 하는 대식세포인 RAW264.7을 사용하였다. 이 단계에서 엠티티 분석과 0.8 μm 트랜스웰 이동 분석법으로 비스페놀A 노출에 의한 암세포와 대식세포의 증식 및 이동 능력을 평가하였고, 이에 관여하는 암세포 내 신호전달기전 분석은 웨스턴블럿을 수행하였다. 실시간 역전사중합효소연쇄반응법과 웨스턴블럿을 수행하여 비스페놀A 노출에 의한 대식세포의 면역기능을 분석하였다. 또한 암세포 및 대식세포를 72시간 배양한 조건부 배지 처리 혹은 0.4 μm 트랜스웰 이용한 공동 배양을 통하여 암세포와 대식세포의 상호작용을 분석하였다. 유방암 초기단계에 대한 종양이식모델은 3주령의 면역 결핍 마우스(BALB/c nude)를 한 달간 비스페놀A에 음수 노출시킨 후 마우스의 2번째 유선지방조직에 루시퍼라제 발현 MCF10DCIS.com 세포를 이식하여 생체발광영상 기법으로 종양의 성장과 전이를 추적하였다. 이후 조직면역 염색을 통해 일차 종양 조직과 종양주변의 림프절 조직에서 대식세포마커인 F4/80과 염증성 M1 마커인 NOS2, 종양친화성 M2 마커인 CD206, 그리고 림프절 내에 전이된 유방암세포를 감지하는 CK5의 발현을 확인하여 종양관련 대식세포의 면역기능과 전이 여부를 분석하였다.

결과: 1. 장기간 저용량의 비스페놀A에 노출된 MCF-7, SK-BR3, MDA-MB-231 세포들의 전사체 발현 변화를 분석한 결과, NKT, NK and T cell activation과 dendritic cell migration 등의 면역기능 변화와 관련된 유전자가 공통적으로 확인됐다. 이러한 결과를 바탕으로 유방암 아형별 환자의 생존율 데이터를 분석하여 비스페놀A에 의한 면역관련 상이 발현 유전자의 발현 증가가 유방암 환자의 생존율 감소와 상관관계를 검증하였다.

2. 마찬가지로 저용량 비스페놀A에 노출된 MCF10DCIS.com 세포의 전사체 분석 결과에서도 면역 관련 변화가 보여졌다. 저용량 비스페놀A 노출은 MCF10DCIS.com 세포의 증식과 이동을 유도하였고, RAW264.7 세포의 이동과

NOS, CD206, arginase−1의 발현을 증가시켜 M1과 M2형의 분극화를 유도하였다. MCF10DCIS.com 세포를 이식한 유방암 마우스 모델에서 저용량의 비스페놀A에 의해 일차암 주변의 종양 관련 대식세포들은 CD206을 발현하는 M2형의 분포도가 유의하게 증가하였으며, 종양의 성장과 림프절 전이가 촉진되었다.

결론: 1. 본 연구결과는 지속적인 저용량 비스페놀A 노출이 각 유방암 아형의 세포 주의 면역조절을 포함하여 다양한 생물학적 기능과 유전자 발현 조절에 다른 영향을 미침을 시사한다.

2. 본 연구결과는 비스페놀A 노출이 대식세포의 종양친화적(protumorigenic) 분극뿐만 아니라 DCIS 세포의 증식 및 이동능력에 영향을 주어 침윤성 유방암으로의 진행을 가속시키는 촉진제 역할을 함을 시사한다.

주요어: 비스페놀A, 유방암, 대식세포 분극화, 전사체 분석, 암 진행

학번: 2015−22030